iScience

CellPress
OPEN ACCESS

Article

MicroRNA-31 induced by *Fusobacterium nucleatum* infection promotes colorectal cancer tumorigenesis

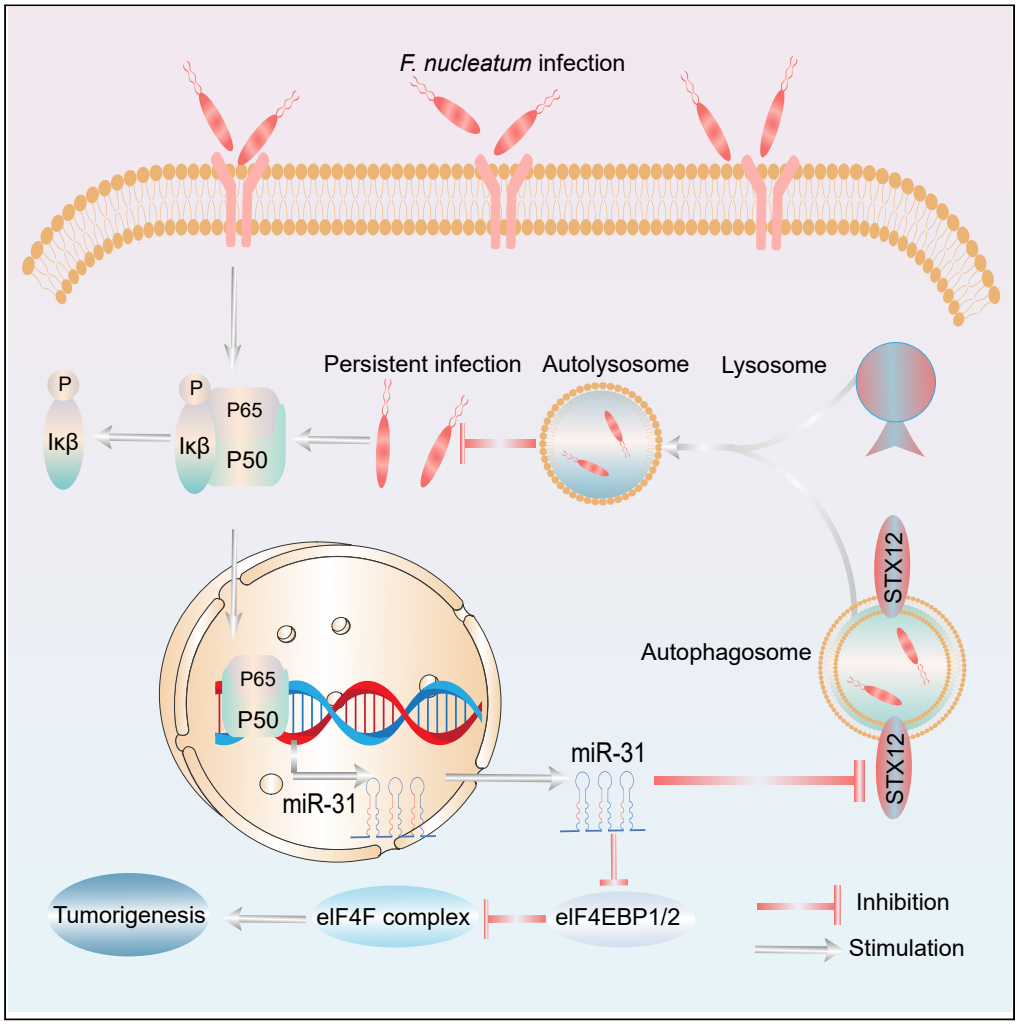

Bin Tang, Xiaoxue Lu, Yanan Tong, ..., Qian Li, Dongzhu Zeng, Xuhu Mao

liqianjane@163.com (Q.L.)
650777@hospital.cqmu.edu.cn (D.Z.)
maoxh2012@hotmail.com (X.M.)

Highlights

Fusobacterium nucleatum promotes autophagy but inhibited autophagic flux

miR-31 enhances the inhibitory effect of *F. nucleatum* on autophagic flux

miR-31 promotes CRC cell proliferation by inhibiting eIF4EBP1/2

miR-31 inhibites *STX12* to block autophagic flux

Tang et al., iScience *26*, 106770
May 19, 2023
https://doi.org/10.1016/j.isci.2023.106770

iScience

CellPress
OPEN ACCESS

Article

MicroRNA-31 induced by *Fusobacterium nucleatum* infection promotes colorectal cancer tumorigenesis

Bin Tang,[1,5] Xiaoxue Lu,[2,5] Yanan Tong,[2,5] Yuyang Feng,[2] Yilan Mao,[4] Guodong Dun,[2] Jing Li,[3] Qiaolin Xu,[3] Jie Tang,[3] Tao Zhang,[3] Ling Deng,[3] Xiaoyi He,[3] Yuanzhi Lan,[3] Huaxing Luo,[3] Linghai Zeng,[3] Yuanyuan Xiang,[3] Qian Li,[2,*] Dongzhu Zeng,[3,*] and Xuhu Mao[2,6,*]

SUMMARY

Persistent *Fusobacterium nucleatum* infection is associated with the development of human colorectal cancer (CRC) and promotes tumorigenicity, but the underlying mechanisms remain unclear. Here, we reported that *F. nucleatum* promoted the tumorigenicity of CRC, which was associated with *F. nucleatum*-induced microRNA-31 (miR-31) expression in CRC tissues and cells. *F. nucleatum* infection inhibited autophagic flux by miR-31 through inhibiting syntaxin-12 (STX12) and was associated with the increased intracellular survival of *F. nucleatum*. Overexpression of miR-31 in CRC cells promoted their tumorigenicity by targeting eukaryotic initiation factor 4F-binding protein 1/2 (eIF4EBP1/2), whereas miR-31 knockout mice were resistant to the formation of colorectal tumors. In conclusion, *F. nucleatum*, miR-31, and STX12 form a closed loop in the autophagy pathway, and continuous *F. nucleatum*-induced miR-31 expression promotes the tumorigenicity of CRC cells by targeting eIF4EBP1/2. These findings reveal miR-31 as a potential diagnostic biomarker and therapeutic target in CRC patients with *F. nucleatum* infection.

INTRODUCTION

Fusobacterium nucleatum (*F. nucleatum*), a Gram-negative anaerobic bacterium, is one of the commensal microbes in the oral microflora and gut microbiota in healthy humans.[1,2] *F. nucleatum* overgrowth has been linked to periodontal and endodontic diseases, as well as inflammatory bowel disease,[2,3] and some cancers including colorectal cancer (CRC).[4,5] There is a higher density of *F. nucleatum* in the tumor tissues and feces of CRC patients compared to the colorectal tissues and feces of healthy controls,[6,7] and *F. nucleatum* is significantly enriched in CRC patients because of the change in gut microbiota.[8] A growing body of research indicates that *F. nucleatum* may be responsible for the development, progression, and possibly pharmaceutical resistance of CRC.[8–11]

Recent research suggests that *F. nucleatum* promotes the development of CRC through a variety of mechanisms, including colonization, invasion, alteration of the host immunological response, and inflammation.[12] Although *F. nucleatum* is typically thought of as an external microorganism, there is evidence that a small portion of it persists inside colorectal epithelial cells and that at least one subset of it has an intraepithelial position.[13–15] It is the intracellular *F. nucleatum* fraction that may represent the source of persistent *F. nucleatum* infection, which may eventually lead to the development of colorectal inflammation and cancer if it is not eliminated by the host's innate immunity.

Autophagy is a crucial intracellular degradation mechanism that recycles macromolecules and damaged cytosolic organelles, as well as an important component of host innate immunity that captures and degrades intracellular microorganisms.[16] Growing evidence from recent research supports the involvement of autophagy in bacterial-associated inflammation and cancer.[17,18] In general, intestinal epithelial autophagy promotes colon cancer growth and progression while inhibiting colitis and colon cancer initiation. A recent study demonstrated that autophagy reduces the survival of *F. nucleatum* as part of an innate immune response.[19] Although *F. nucleatum* can induce autophagosomes in colorectal epithelial cells, it is still able to multiply in these cells.[10] These results suggest that *F. nucleatum* can affect autophagic flux, which is the term used to describe the complete autophagic process, including the inclusion of cargo inside the

[1]Department of Clinical Laboratory, Chongqing University Jiangjin Hospital, School of Medicine, Chongqing University, Jiangjin, Chongqing 402260, China

[2]Department of Clinical Microbiology and Immunology, College of Pharmacy and Medical Laboratory, Army Medical University (Third Military Medical University), Chongqing 400038, China

[3]Department of General Surgery, The Third Affiliated Hospital of Chongqing Medical University, Chongqing 401120, China

[4]Class of 2021 undergraduate, Nursing College of Chongqing Medical University, Chongqing 400016, China

[5]These authors contributed equally

[6]Lead contact

*Correspondence: liqianjane@163.com (Q.L.), 650777@hospital.cqmu.edu.cn (D.Z.), maoxh2012@hotmail.com (X.M.)

https://doi.org/10.1016/j.isci.2023.106770

autophagosome, the transport of cargo to lysosomes, and the subsequent breakdown and release of the resultant macromolecules back into the cytosol. However, it is still unclear exactly how *F. nucleatum* interferes with the host's autophagic flux.

MicroRNAs (miRNAs) are involved in the development and progression of several cancers through negatively regulating gene expression at the post-transcriptional level.[20–22] Moreover, miRNAs also are crucial in the complex interaction between a host and a bacterial pathogen, whether as a component of the human immune response to regulate the infection or as a bacterium-directed molecular strategy to take advantage of the host pathways.[23,24] Therefore, microorganisms have evolved multiple strategies including the regulation of host miRNAs to counteract autophagy, which also plays an important role in combating bacterial infection.[25] Many studies have confirmed that miRNAs are involved in the process by which bacterial pathogens antagonize autophagy.[26,27] For example, miR-31 affects CRC by inhibiting autophagy in cancer-associated fibroblasts and cells.[28,29] However, whether miR-31 is involved in *F. nucleatum*-induced autophagy in colorectal epithelial cells and whether miR-31 contributes to the persistence of *F. nucleatum* infection are largely unclear.

This study investigated the role of miR-31 in *F. nucleatum*-induced CRC tumorigenicity and the persistence of *F. nucleatum* infection in CRC patients, as well as the underlying molecular mechanisms.

RESULTS

F. nucleatum is associated with CRC and promotes tumorigenicity in C57BL/6J mice

First, we investigated the association between *F. nucleatum* abundance and CRC by detecting *F. nucleatum* DNA levels in fresh-frozen cancer tissues from 30 CRC patients and colorectal polyp tissues from 30 patients with colorectal polyps. *F. nucleatum* DNA levels (Figure 1A) were significantly higher in cancer tissues than in polyp tissues. In addition, the positive rate of *F. nucleatum* was similar between patients with colorectal polyps and those with CRC and was as high as >70%, indicating that *F. nucleatum* infection is equally associated with the occurrence and development of colorectal polyps and CRC (Table S1). Moreover, an increased amount of *F. nucleatum* was associated with shorter recurrence-free survival (RFS, Figure 1B), depth of invasion ($P < 0.001$), and tumor stage (tumor-node-metastasis [TNM], $P < 0.001$) and CRC formation and progression (Table S2). *F. nucleatum* infection significantly increased the tumor number and caused obvious pathological changes in the colorectum of C57BL/6J mice following azoxymethane (AOM)/dextran sodium sulfate (DSS) treatment and administration of *F. nucleatum*, *Escherichia coli* DH5α, or PBS (negative control [NC]) for 20 weeks (Figures 1C and 1D), indicating that *F. nucleatum* plays a supporting role in colorectal tumorigenesis. Additionally, 5-ethynyl-20′-deoxyuridine (EdU) experiments demonstrated that *F. nucleatum* infection greatly accelerated cell proliferation as compared to *E. coli* DH5α infection or the NC (PBS) (Figure 1E). Taken together, these results suggest that *F. nucleatum* infection not only contributes to the initiation of CRC but also to the development of CRC.

Autophagic flux is inhibited in response to *F. nucleatum* infection

To determine whether *F. nucleatum* modulates autophagy, we observed the structure of autophagosomes using transmission electron microscopy (TEM) in HCT116 cells infected with *F. nucleatum*. The bacterium was observed in the cytoplasm and double-membrane compartments (Figure 2A), indicating the generation of autophagosomes in the infected cells. Given the importance of the autophagy pathway in carcinogenesis, the expression levels of autophagy elements (MAP1LC3B-I/II and SQSTM1) were further measured in CRC tissues with or without *F. nucleatum* infection. In contrast to the expression shown in the *F. nucleatum*-negative CRC tissues, the expression of MAP1LC3B-II and SQSTM1 was much higher in the *F. nucleatum*-positive CRC tissues (Figure 2B). Further experiments in HCT116 cells expressing mGFP-LC3 fusion protein indicated that *F. nucleatum* infection or rapamycin increased the accumulation of MAP1LC3B-positive autophagosomes in HCT116 cells (Figure 2C). Moreover, activation of autophagy by rapamycin significantly inhibited the intracellular survival of *F. nucleatum* (Figure 2D). To observe autophagic flux after *F. nucleatum* infection, we established HCT116 cells expressing mRFP-GFP-LC3. As shown in Figure 2E, Baf-A1 or *F. nucleatum* blocked the fusion between autophagosomes and lysosomes, while rapamycin promoted the formation of autolysosomes. We also measured the expression levels of MAP1LC3B-I/II and SQSTM1 in HCT116 cells following *F. nucleatum* infection. An increase in the expression of MAP1LC3B-II and accumulation of insoluble and total SQSTM1 were observed in HCT116 cells infected with *F. nucleatum* at 2, 4, 6, 12, and 24 h post-infection compared to uninfected cells (Figure 2F). Furthermore, blocking autophagic flux using Baf-A1 inhibited

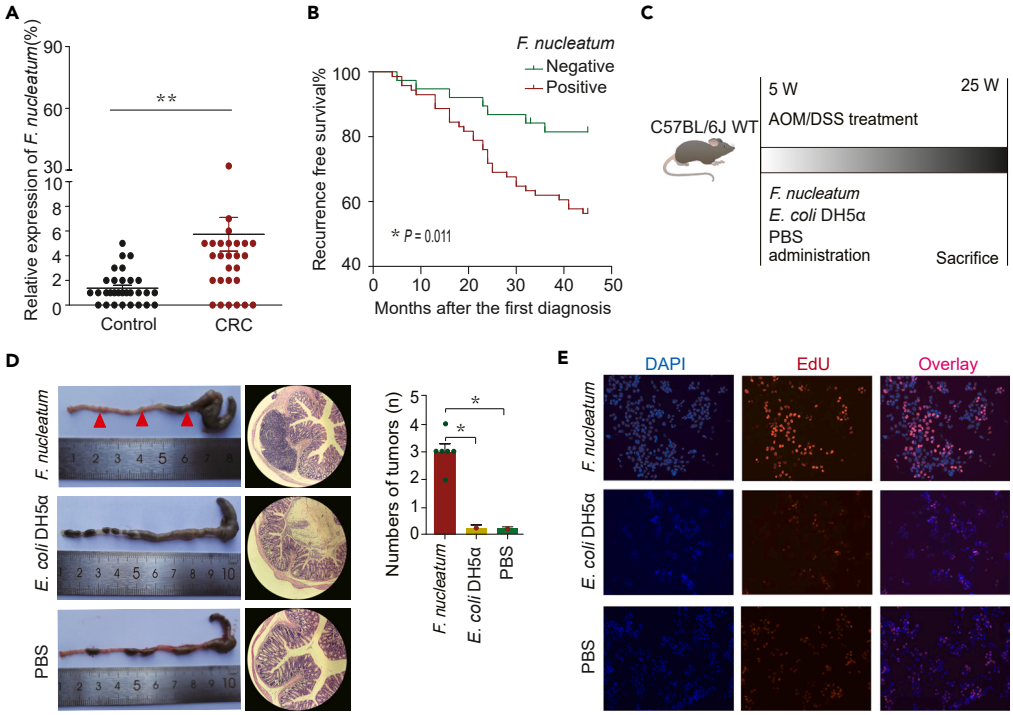

Figure 1. *F. nucleatum* infection contributes to the tumorigenicity of CRC

(A) RT-qPCR analysis detected the expression levels of *F. nucleatum* in the CRC tissues (CRC, n = 30) and the colorectal polyp tissues from patients (control, n = 30).

|(B) Kaplan-Meier analysis that more *F. nucleatum* was linked to a poor RFS for CRC patients (n = 109).

(C) Five-week-old C57BL/6J mice were administered *F. nucleatum* or *E. coli* DH5α or PBS and sacrificed after AOM/DSS treatment for 20 weeks.

(D) Representative image, numbers of tumors, and H&E staining of a colon of C57BL/6J mice infected with *F. nucleatum*, *E. coli*, or PBS.

(E) EdU staining of the proliferation of HCT116 cells infected with *F. nucleatum*, *E. coli*, or PBS. *p < 0.05; **p < 0.01.

MAP1LC3B-II generation and insoluble and total SQSTM1 accumulation (Figure 2G). Not only that but *F. nucleatum* infection also increased the expression of soluble SQSTM1 and SQSTM1 mRNA in HCT116 cells (Figures 2F and 2G). These results indicated that *F. nucleatum* could induce the initiation of autophagy but impair autophagic flux.

F. nucleatum infection upregulates miR-31 expression in CRC tissues and cells, and miR-31 enhances the inhibitory effect of *F. nucleatum* on *autophagy* and induces tumorigenicity

We previously identified differentially expressed miRNAs in CRC tissues with or without *F. nucleatum* infection,[30] and Yang Y et al. also identified differentially expressed miRNAs in four CRC cell lines (HCT116, HT29, LoVo, and SW480) infected with *F. nucleatum*.[31] Based on these available data, we identified two miRNAs responsive to *F. nucleatum* infection, with a 5.67-fold increase of hsa-miR-31-5p (hereinafter referred to as miR-31) and a 1.29-fold decrease of hsa-miR-4443 (Figure 3A). In addition, miR-31 expression was significantly higher in *F. nucleatum*-positive CRC tissues (Fn+ CRC) than in *F. nucleatum*-positive paracancerous samples (Fn^+ control) (Figure 3B), while there was no significant difference in the expression of hsa-miR-4443 (Figure S1A). *In vitro*, *F. nucleatum* infection significantly raised the expression of miR-31 in four CRC cell lines (SW480, HT29, LoVo, and HCT116), as well as the normal colonic epithelial cell line (NCM460) (Figure 3C), and the expression of miR-31 was similarly time- and *F. nucleatum*-dose-dependent (Figures S1B and S1C).

To further demonstrate the association between miR-31 expression and *F. nucleatum* infection, miR-31 transcript expression was measured in fresh-frozen cancer tissues from 30 CRC patients and colorectal polyp tissues from 30 patients with colorectal polyps (Table S1). miR-31 levels were higher in cancer tissues than in colorectal polyp tissues (Figure 3D) and were positively correlated with *F. nucleatum* numbers in cancer tissues (Figure 3E). In a large cohort of 109 CRC patients including the aforementioned 30 CRC patients (Table S2),

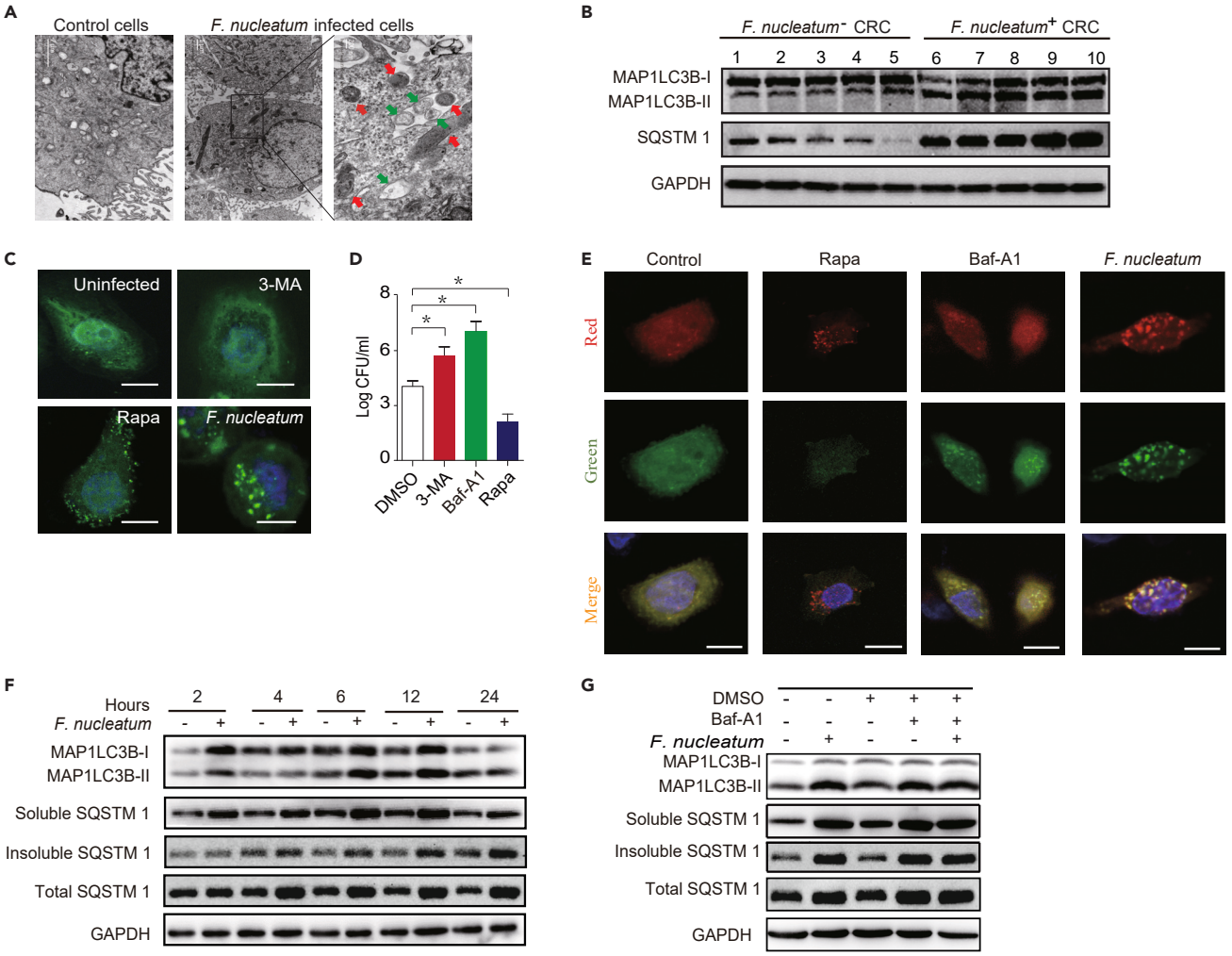

Figure 2. Autophagic flux is inhibited in response to *F. nucleatum* infection

(A) Autophagosomes (green arrows) and bacteria (red arrows) were observed by transmission electron microscopy in HCT116 cells co-cultured with *F. nucleatum* (MOI = 100).

(B) Western blotting detected the expression of MAP1LC3B-I/II and SQSTM1 in colorectal tissues from *F. nucleatum*-positive CRC patients (n = 5) and *F. nucleatum*-negative CRC patients (n = 5).

(C) Quantification of GFP-MAP1LC3B puncta, representing autophagosomes. HCT116 cells with transiently expressing GFP-LC3 fusion protein were co-cultured with an autophagy activator, rapamycin (100 nM), an inhibitor, 3-MA (2 mM) or *F. nucleatum* (MOI = 100) for 6 h. Bar scale, 5 μm.

(D) Gentamicin protection assay showed the intracellular survival of *F. nucleatum* in HCT116 cells after treatment with one of the autophagy inhibitors, 3-MA (2 mM) and bafilomycin A1 (Baf-A1, 10 nM), or an activator, rapamycin (100 nM). (E) HCT116 cells stably expressing the mRFP-EGFP-LC3 fusion protein were co-cultured with rapamycin, Baf-A1, or *F. nucleatum* at 24 h. Bar scale, 5 μm.

(F) The expression of autophagy elements, MAP1LC3B-I/II and SQSTM1, in HCT116 cells co-cultured with *F. nucleatum* at 2, 4, 6, 12, and 24 h post-infection, as detected by Western blotting.

(G) The expression of MAP1LC3B-I/II and insoluble/soluble/total SQSTM1 in HCT116 cells co-cultured with *F. nucleatum* in the presence of the activator Baf-A1.

the prognostic value of miR-31 in CRC patients with or without *F. nucleatum* infection was assessed. High levels of miR-31 were connected to poor RFS (Figure 3F). More significantly, the group with both *F. nucleatum* infection and a high level of miR-31 expression had the worst prognosis when patients were separated into three groups based on the status of *F. nucleatum* infection and the levels of miR-31 expression (Figure 3G).

The effect of miR-31 on *F. nucleatum*-modulated autophagy pathway was investigated. In HCT116 cells infected with *F. nucleatum*, a miR-31 mimic significantly increased MAP1LC3B-II conversion and SQSTM1 accumulation, while a miR-31 inhibitor attenuated the changes (Figure 3H). Laser scanning confocal

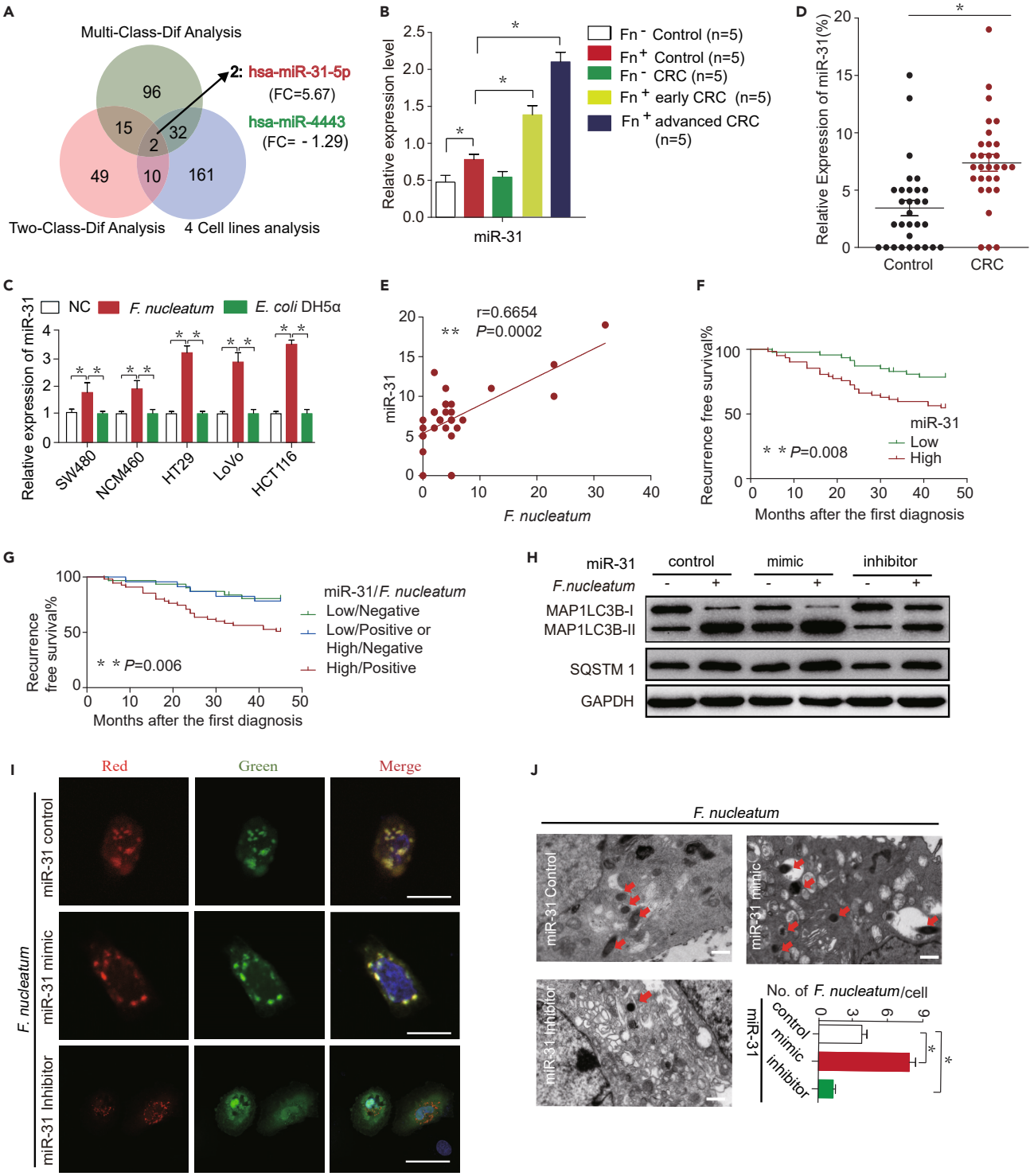

Figure 3. *F. nucleatum* infection upregulates miR-31 expression in CRC tissues and cell lines and miR-31 promotes *F. nucleatum*-induced autophagic flux inhibition

(A) Schematic diagram showing the identification of miRNAs related to both CRC and *F. nucleatum* infection (hsa-miR-31-5p [miR-31] and hsa-miR-4443).

(B) The expression of miR-31 was detected by RT-qPCR in clinical specimens, including *F. nucleatum*-negative (Fn^-) control (n = 5), *F. nucleatum*-positive (Fn^+) control (n = 5), Fn^- CRC (n = 5), Fn^+ early CRC (n = 5), and Fn^+ advance CRC (n = 5) tissues.

(C) RT-qPCR was used to determine the expression of miR-31 in 5 CRC cell lines (SW480, LoVo, HCT116, HT29, and NCM460) 24 h after *F. nucleatum* or *E. coli* infection.

Figure 3. *Continued*

(D) RT-qPCR analysis detected the expression level of miR-31 in the CRC tissues (CRC, n = 30) and colorectal polyp tissues from patients (control, n = 30).

(E) The correlation between *F. nucleatum* abundance and miR-31 expression levels was examined by Spearman correlation analysis (*F. nucleatum*/miR-31, R = 0.6654, p = 0.0002).

(F and G) Kaplan-Meier survival curve for 109 CRC patients with both *F. nucleatum* DNA level and high miR-31 expression (log rank [Mantel-Cox] test).

(H) HCT116 cells were transfected with a miR-31 mimic, an inhibitor or a control. After co-culture with *F. nucleatum*, autophagy elements (MAP1LC3B-I/II and SQSTM1) were detected by Western blotting.

(I) HCT116 cells stably expressing mRFP-EGFP-LC3 fusion protein were transfected with a miR-31 mimic, an inhibitor or a control, and LSCM was used to detect the mRFP-EGFP-LC3 fusion protein in cells after infection with *F. nucleatum* for 6 h. Bar scale, 5 μm.

(J) The intracellular survival of *F. nucleatum* in HCT116 cells following transfection with the miR-31 mimic, inhibitor, or control was examined using transmission electron microscopy. Bar scale, 0.5 nm.

microscope (LSCM) of HCT116 cells transfected with the miR-31 mimic revealed an increase in the number of mRFP-GFP-LC3 puncta after 6 h of infection with *F. nucleatum*, while the miR-31 inhibitor reversed the block of autophagic flux induced by *F. nucleatum* (Figure 3I). TEM showed that, compared to the miR-31 control, the miR-31 mimic significantly increased the intracellular survival of *F. nucleatum*, while the miR-31 inhibitor significantly decreased intracellular survival (Figure 3J). These results indicate that miRNA-31 enhances the inhibitory effect of *F. nucleatum* on autophagic flux, thus contributing to the persistent infection of *F. nucleatum* in CRC cells.

Next, we further determined whether *F. nucleatum* promotes tumorigenicity in a miR-31-dependent manner using miR-31$^{-/-}$ mice. Both miR-31^{wt} and miR-31$^{-/-}$ mice were initially administered *F. nucleatum* and then subjected to treatment with AOM/DSS (dextran sodium sulfate) (Figure 4A). As shown in Figures 4B and 4C, there were fewer tumors in the colorectum of miR-31$^{-/-}$ mice than of miR-31^{wt} mice. Furthermore, miR-31$^{-/-}$ mice survived longer than miR-31^{wt} mice (Figure 4D). Further *in vivo* experiments in xenograft mice bearing miR-31 overexpressed/knockdown HCT116 cells showed that tumor weight and volume were significantly increased in the miR-31 overexpression group but were decreased in the miR-31 knockdown group compared with the respective control group (Figures 4E and 4F). In addition, expression of the proliferation marker, Ki-67, was upregulated in xenografts overexpressing miR-31 and downregulated in xenografts with miR-31 knockdown (Figure 4G). Finally, the effects of miR-31 overexpression/knockdown on cell proliferation of HCT116 and LoVo cells were investigated. The overexpression of miR-31 significantly promoted HCT116 and LoVo cell growth, whereas the knockdown of miR-31 inhibited cell growth (Figure 4H). These results indicate that *F. nucleatum* infection induces tumorigenicity, at least in part, through miR-31.

STX12, eIF4EBP1, and *eIF4EBP2* are direct targets of miR-31

To identify potential target genes of miR-31 in CRC cells, cDNA microarray analyses showed that 10 genes were downregulated in HCT116 cells with miR-31 overexpression (Figure 5A). After combination with the TargetScan prediction, MiRnada, miRDB, Gene Ontology (GO) annotation, and target of microarray verification (tissues and cells), STX12, which belongs to the soluble N-ethylmaleimide-sensitive factor attachment protein receptors (SNARE) family and is the only gene closely related to autophagy and eIF4EBP1 and eIF4EBP2,[32] which are related to tumor progression,[33,34] were selected for further analyses (Figure 5B).

To determine whether miR-31 directly regulates STX12/eIF4EBP1/2 expression through its 3′-UTR, we introduced wild-type (WT) or mutant (MT) 3′-UTR of STX12, eIF4EBP1, and eIF4EBP2 into luciferase reporter plasmids (Figure 5C). A miR-31 mimic, an inhibitor, or an NC was transiently transfected into HEK293 cells together with luciferase constructs. The reporter genes STX12, eIF4EBP1, and eIF4EBP2 carrying WT 3′-UTRs were strongly affected by miR-31 overexpression or inhibition, which decreased or raised their luciferase activity, respectively. However, cells transfected with MT 3′UTR did not exhibit any inhibitory effects (Figure 5D). In addition, the miR-31 mimic lowered the mRNA and protein levels of STX12 and eIF4EBP1/2 while increasing them with the inhibitor in HCT116 cells (Figures 5E and 5F) and LoVo cells (Figures S2A and S2B). These findings imply that miR-31 directly targets STX12, eIF4EBP1, and eIF4EBP2.

miRNA-31 promotes CRC cell proliferation by inhibiting eIF4EBP1/2

Next, we investigated whether *F. nucleatum* can lead to reduce the expression of eIF4EBP1/2 through miR-31, and triggers CRC. As shown in Figure 6A, *F. nucleatum* reduced the expression of eIF4EBP1/2. The effect was reversed by the miR-31 inhibitor but enhanced by the miR-31 mimic. Likewise, in the presence of *F. nucleatum* infection, the expression of eIF4EBP1/2 was significantly increased in miR-31$^{-/-}$ mice compared with miR-31 ^{wt} mice (Figure 6B). Moreover, eIF4EBP1/2 expression was downregulated in CRC

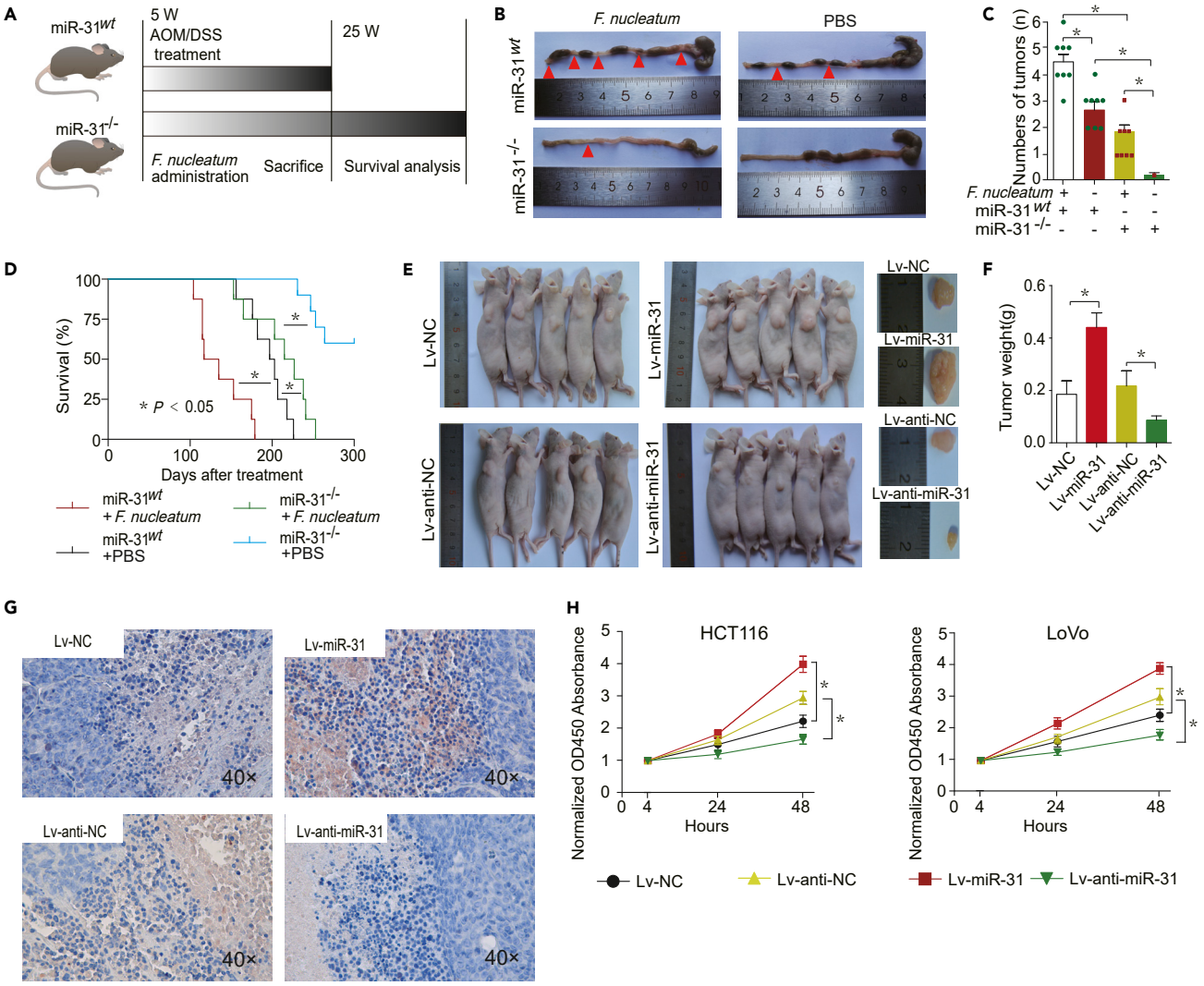

Figure 4. MiRNA-31 promotes tumorigenicity of CRC

(A) Both miR-31 WT (miR-31 ^{wt}) and miR-31$^{-/-}$ mice were administrated with or without *F. nucleatum* and subjected to AOM/DSS treatment for 20 weeks. The colon appearance and tumor number were observed, and colons were subjected to Western blotting.

(B and C) A representative colon and the number of tumors in the miR-31 ^{wt} and miR-31$^{-/-}$ mice with or without *F. nucleatum* infection.

(D) Kaplan-Meier survival curve for miR-31$^{-/-}$ and miR-31 ^{wt} mice with or without *F. nucleatum* infection (n = 8 per group by log rank [Mantel-Cox] test).

(E and F) Nude mice were subcutaneously injected HCT116 cells transfected with Lv-NC, Lv-miR-31, Lv-*anti*-NC, or Lv-anti-miR-31, n = 5) and the tumor weight and volume in xenograft tumor tissues.

(G) Immunostaining for Ki-67 (400×) in xenograft tumor tissues.

(H) HCT116 and LoVo cells were infected with lentivirus Lv-NC, Lv-miR-31, Lv-anti-NC or Lv-anti-miR-31. The cell proliferation rates were evaluated by the CCK-8 assay at 4, 24, and 48 h after treatment (*p < 0.05).

tissues (Figure 6C). In addition, Spearman's correlation analysis showed that decreased expression levels of eIF4EBP1/2 were correlated with high levels of miR-31 expression in human clinical specimens (Figure 6C).

To further confirm that miR-31-mediated dysregulation of eIF4EBP1/2 can promote CRC cell proliferation, we first used small interfering RNA (siRNA) to reduce the expression of eIF4EBP1/2 in HCT116 cells (Figure 6D). Knockdown of eIF4EBP1/2 subsequently increased CRC cell proliferation (Figure 6E), which was similar to the promoting effect of miR-31 on cancer progression. Next, we re-introduced eIF4EBP1/2 via a eukaryotic expression vector into HCT116 cells that overexpressed miR-31 (Figure 6F). The ectopic expression of eIF4EBP1/2 restored the inhibitory effect on cell proliferation (Figure 6G) induced by miR-31. In addition, to further confirm that miR-31 regulates the intracellular survival of *F. nucleatum in vivo*,

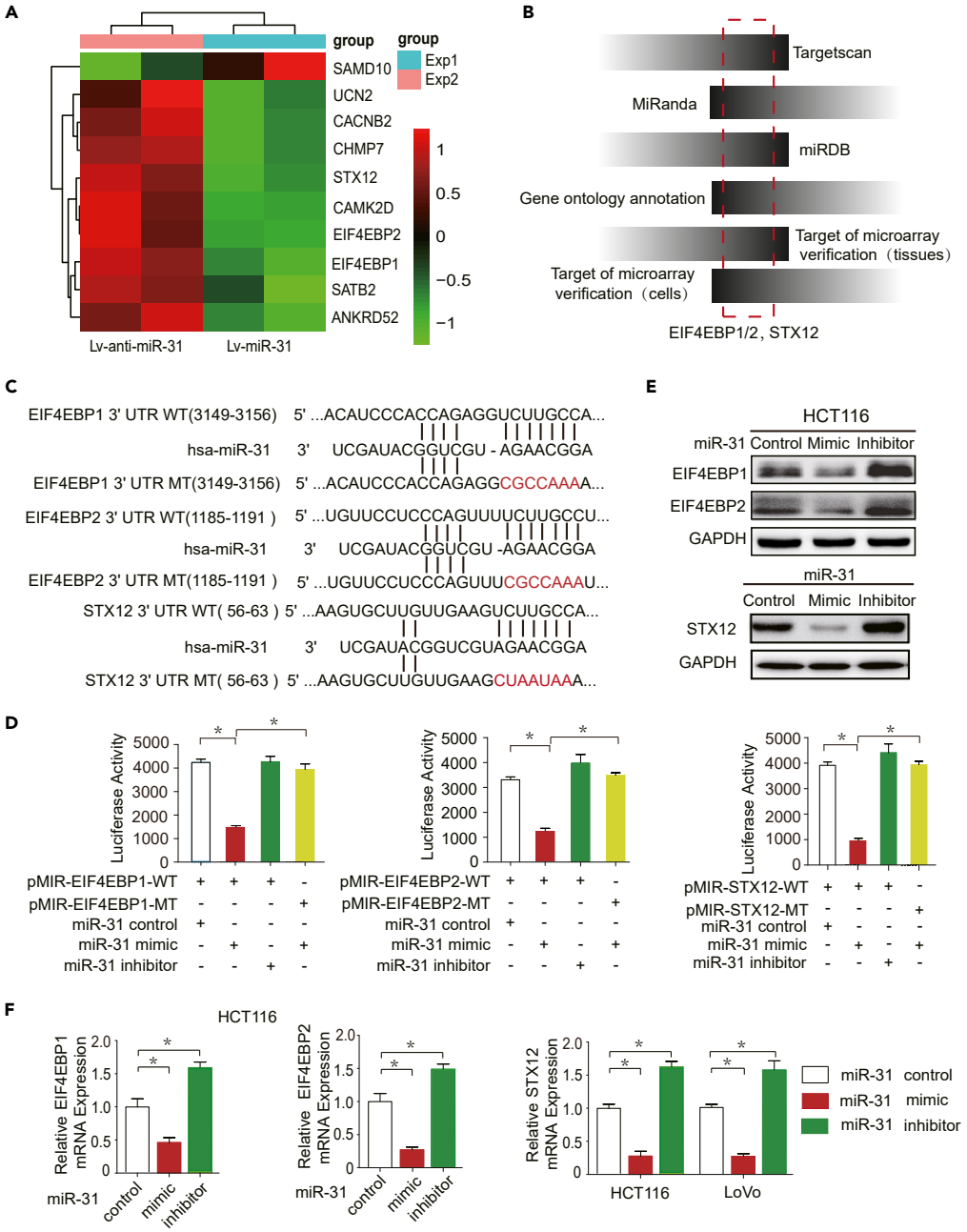

Figure 5. STX12, eIF4EBP1, and eIF4EBP2 are direct targets of miR-31

(A) The differentially expressed mRNAs among HCT116 cells transfected with Lv-miR-31, Lv-NC, Lv-anti-miR-31, or Lv-anti-NC, as identified by microarray.

(B) eIF4EBP1/2 and STX12 were identified as the direct targets of miR-31 as detected and verified by the TargetScan prediction, MiRnada, miRDB, GO annotation, and target of microarray, respectively.

(C) The region of the human eIF4EBP1/2 and STX12 mRNA 3′UTR was predicted to be targeted by miR-31 (TargetScan 7.2).

(D) Luciferase reporter plasmids were generated with either WT or MT miR-31 binding sites in 3′-UTR of eIF4EBP1/2 and STX12. The activity of the luciferase constructs was evaluated and normalized to the activity of Renilla luciferase after transfecting HEK293T cells with a miR-31 mimic, an inhibitor, or a control.

(E and F) HCT116 cells were transfected with the mimic or the inhibitor of miR-31. After co-culture with *F. nucleatum* for 4 h, the mRNA and protein expression of eIF4EBP1/2 and STX12 was detected by RT-qPCR and Western blotting, respectively.

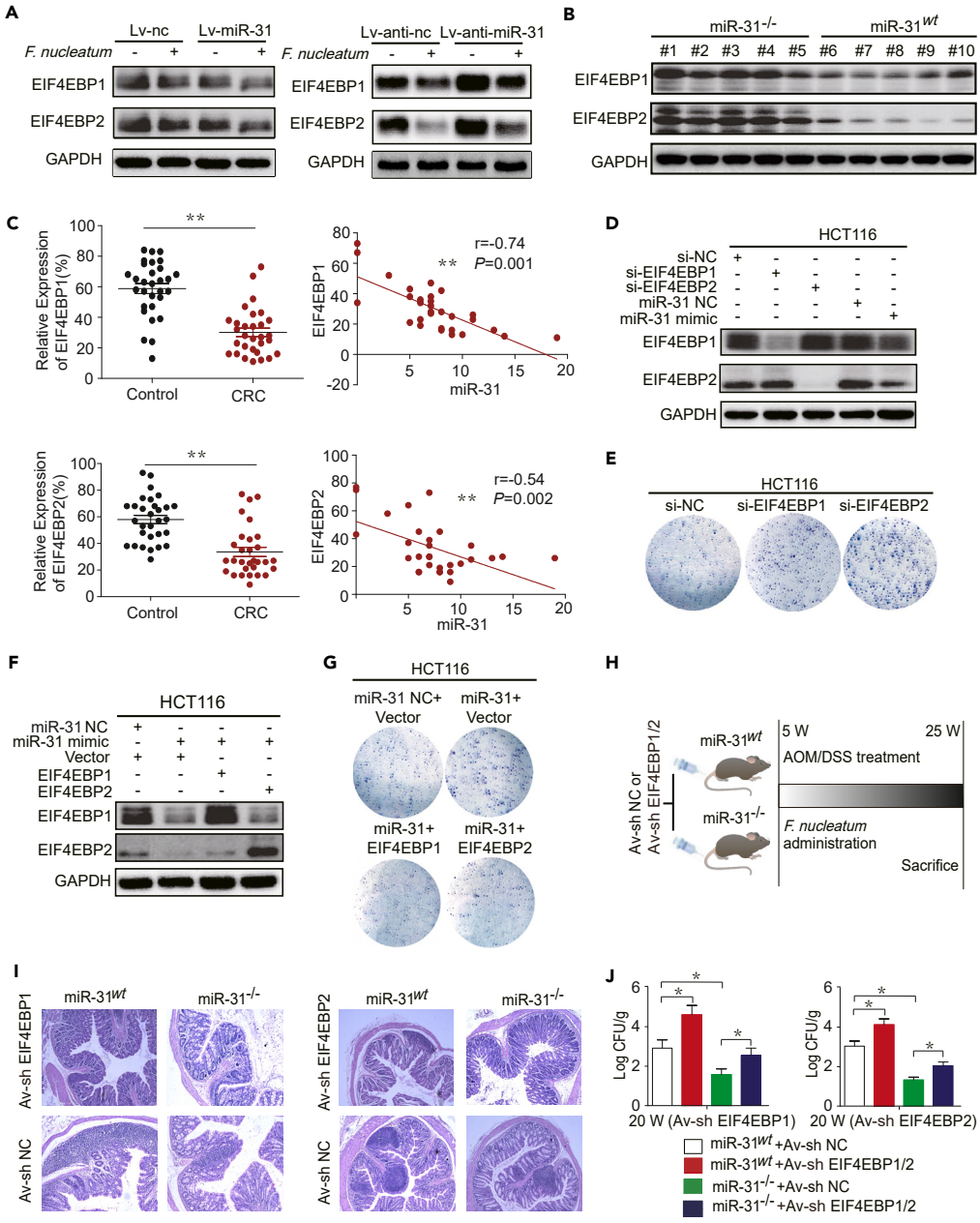

Figure 6. miRNA-31 promotes *F. nucleatum*-induced CRC cell proliferation by targeting eIF4EBP1/2

(A) After HCT116 cells were infected with *F. nucleatum* for 24 h, the protein expression of eIF4EBP1/2 was detected by Western blotting. eIF4EBP1/2 expression was downregulated by miR-31 overexpression but upregulated by miR-31 inhibition in HCT116 cells.

(B) In the presence of *F. nucleatum* infection, the protein expression levels of eIF4EBP1/2 in colon tissues were significantly downregulated in miR-31 ^{wt} mice (n = 5), compared with that in miR-31$^{-/-}$ mice.

(C) mRNA expression of eIF4EBP1/2 was increased in CRC tissues as detected by RT-qPCR analysis (left), which was negatively associated with miR-31 expression (right).

(D) HCT116 cells were transiently transfected with a miR-31 mimic, a miR-31 control, si-eIF4EBP1/2, or si-control (si-NC) for 24 h. The protein levels of eIF4EBP1/2 were determined by Western blotting.

(E) eIF4EBP1 or eIF4EBP2 knockdown enhanced the colony-forming ability of CRC cells (HCT116 cell).

(F) HCT116 cells were transiently co-transfected with a miR-31 mimic or a eukaryotic expression plasmid of eIF4EBP1 or eIF4EBP2 for 24 h. The protein levels of eIF4EBP1/2 were determined by Western blotting. Vector is pcDNA3.1 plasmid.

(G) Ectopic expression of eIF4EBP1 or eIF4EBP2 abrogated miR-31-dependent promotion of colony formation in CRC cells (HCT116 cell).

Figure 6. *Continued*
(H) Both miR-31^{wt} and miR-31$^{-/-}$ mice were initially injected with Av-sh-NC, Av-sh eIF4EBP1, or eIF4EBP2 via the caudal vein and then infected with *F. nucleatum* for 20 weeks.
(I) Representative images of H&E staining of the colonic epithelium from miR-31^{wt} and miR-31$^{-/-}$ mice.
(J) The colonization of *F. nucleatum* in colorectal tissues of miR-31^{wt} mice was more than one in miR-31$^{-/-}$ mice and knockdown of eIF4EBP1 or eIF4EBP2 increased the colonization of *F. nucleatum* in colorectal tissues of miR-31^{wt} or miR-31$^{-/-}$ mice. *$p < 0.05$.

miR-31^{wt} and miR-31$^{-/-}$ mice were first treated with Av-sh-NC and Av-sh-eIF4EBP1/2 and then with *F. nucleatum* and AOM/DSS (Figure 6H). An increased number of inflammatory cells infiltrated into the colorectal tissues of miR-31^{wt} mice, compared with miR-31$^{-/-}$ mice, and Av-sh-eIF4EBP1/2 inhibited inflammatory cells infiltrated into the colorectal tissues of miR-31^{wt} and miR-31$^{-/-}$ mice (Figure 6I). In agreement with the tissue inflammation, the gentamicin protection assay also showed that miR-31 knockout significantly inhibited the survival and colonization of *F. nucleatum* in mouse colorectal cells, which was reversed by Av-sh-eIF4EBP1/2 (Figure 6J). These findings collectively imply that *F. nucleatum* stimulates CRC cell proliferation via the miR-31/eIF4EBP1/2 pathway.

miR-31 inhibits STX12 to block *the* fusion of autophagosomes with lysosomes during *F. nucleatum* infection

To determine if STX12 is involved in the enhancement by miR-31 of the inhibitory effect of *F. nucleatum* on autophagic flux, first, the effect of *F. nucleatum* on STX12 expression was investigated. As shown in Figure 7A, miR-31 mimic could inhibit the expression of STX12, while knockdown of miR-31 reversed the downregulation of STX12 in *F. nucleatum*-infected HCT116 cells. The expression of STX12 was significantly reduced in WT mice compared with miR-31$^{-/-}$ mice (Figure 7B). Additionally, compared to *F. nucleatum*-negative CRC tissues, the expression of STX12 was also reduced in *F. nucleatum*-infected CRC tissues (Figure 7C).

To further understand the functional consequences of STX12 in *F. nucleatum* infection, we treated HCT116 cells with Lv-sh-STX12 or Lv-sh-NC after *F. nucleatum* inoculation. Notably, cells treated with Lv-sh-STX12 in the presence of *F. nucleatum* increased MAP1LC3B-II generation and SQSTM1 accumulation as compared to *F. nucleatum* infection alone (Figure 7D). Lv-sh-STX12 or *F. nucleatum* blocked the fusion between autophagosomes and lysosomes (Figure 7E). Additionally, TEM showed that STX12 silencing resulted in significantly increased intracellular survival of *F. nucleatum* in HCT116 cells (Figure 7F). These results suggested that STX12 promoted autophagic flux impaired by *F. nucleatum*.

To confirm that miR-31 regulates the fusion of autophagosomes and lysosomes through targeting STX12, HCT116 cells transfected with Lv-sh-NC or Lv-sh-STX12 were treated with a miR-31 mimic or an inhibitor. As shown in Figure 7G, the miR-31 inhibitor inhibited the intracellular survival of *F. nucleatum* in HCT116 cells, while STX12 knockdown blocked the effect. In addition, to further confirm that miR-31 regulates the intracellular survival of *F. nucleatum in vivo*, miR-31^{wt} and miR-31$^{-/-}$ mice were first treated with Av-sh-NC and Av-sh-STX12 and then with *F. nucleatum* and AOM/DSS (Figure 7H). A large number of inflammatory cells infiltrated into the colorectal tissues of both miR-31^{wt} and miR-31$^{-/-}$ mice treated with Av-sh-STX12. Whereas few inflammatory cells infiltrated WT mice treated with Av-sh-NC, and the colorectal tissues of miR-31$^{-/-}$ mice treated with Av-sh-NC were relatively intact or infiltrated with few inflammatory cells (Figure 7I). In agreement with the tissue inflammation, the gentamicin protection assay showed that miR-31 knockout significantly inhibited the survival and colonization of *F. nucleatum* in mouse colorectal cells, which was reversed by Av-sh-STX12 (Figure 7J). Collectively, these results suggest that miR-31 inhibits autophagic flux-mediated elimination of intracellular *F. nucleatum* by targeting STX12.

F. nucleatum upregulates miR-31 expression through NF-κB

To investigate the mechanism by which *F. nucleatum* controls miR-31 expression, we screened 1,074 differentially expressed mRNAs to explore the signaling pathways that are activated in *F. nucleatum*-associated CRC. Based on these differentially expressed mRNAs, KEGG pathway enrichment analysis revealed that *F. nucleatum* affected multiple signaling pathways in CRC tissues, including the Toll-like receptor signaling pathway, proteoglycans in cancer, and the IL-17 signaling pathway (Figure 8A). These results indicated that *F. nucleatum* infection could significantly stimulate the inflammatory response pathway. In inflammation and cancer, the NF-κB family of transcription factors is increasingly recognized as a crucial player.[35] After *F. nucleatum* infection, the phosphorylation level of NF-κB subunit p65 was substantially upregulated in the

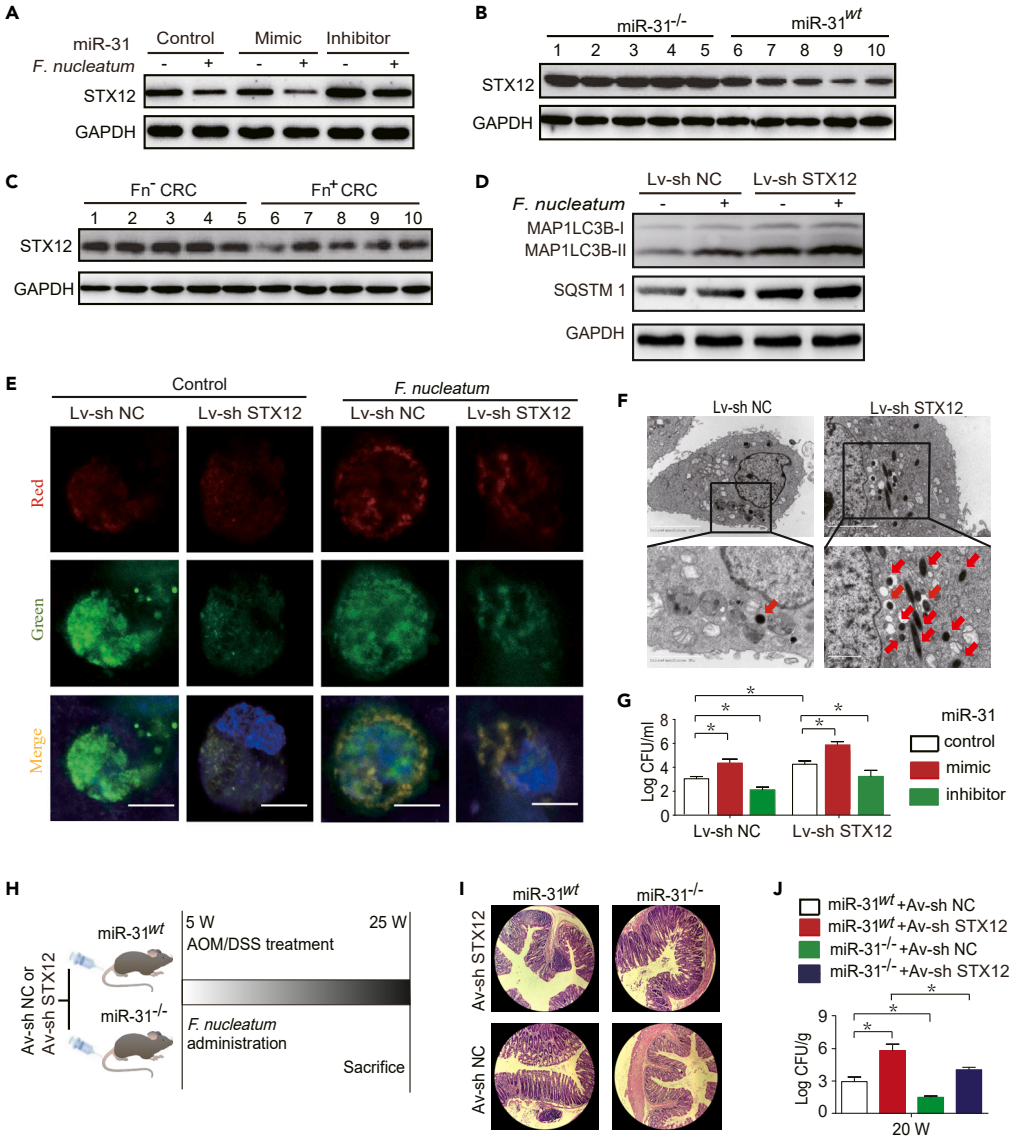

Figure 7. miR-31 inhibits STX12 to block the fusion of autophagosomes with lysosomes during *Fusobacterium nucleatum* infection

(A) The protein expression of STX12 in miR-31 overexpressed or inhibited HCT116 cells infected with *F. nucleatum* (MOI = 100:1) for 6 h.

(B) Western blotting detected the protein expression of STX12 in *F. nucleatum*-infected miR-31^{wt} or miR-31$^{-/-}$ mice tissues (n = 5 per group).

(C) The protein expression of STX12 was detected by Western blotting in *F. nucleatum*-positive CRC tissues (Fn^{+} CRC, n = 5) and *F. nucleatum*-negative CRC tissues (Fn^{-} CRC, n = 5).

(D and E) HCT116 cells were treated with Lv-sh-NC or Lv-sh-STX12, and then infected with *F. nucleatum* (MOI = 100). The expression of MAP1LC3B-I/II and SQSTM1 was detected by Western blotting, and the mRFP-EGFP-LC3 fusion protein was detected by laser scanning confocal microscopy (LSCM).

(F) After pretreatment with Lv-sh-NC or Lv-sh-STX12, HCT116 cells were infected with *F. nucleatum* (MOI = 100:1) for 6 h. Then the intracellular survival of *F. nucleatum* in HCT116 cells were detected by TEM.

(G) HCT116 cells treated with Lv-sh-STX12 were transiently transfected with a miR-31 mimic or an inhibitor, and then infected with *F. nucleatum*, the intracellular survival of *F. nucleatum* was detected 6 h post-infection.

(H) Both miR-31^{wt} and miR-31$^{-/-}$ mice were initially injected with Av-sh-NC or Av-sh-STX12 via the caudal vein and then infected with *F. nucleatum* for 20 weeks.

(I) Representative images of H&E staining of the colonic epithelium from miR-31^{wt} and miR-31$^{-/-}$ mice.

(J) The colonization of *F. nucleatum* in colorectal tissues of miR-31^{wt} and miR-31$^{-/-}$ mice. *p < 0.05.

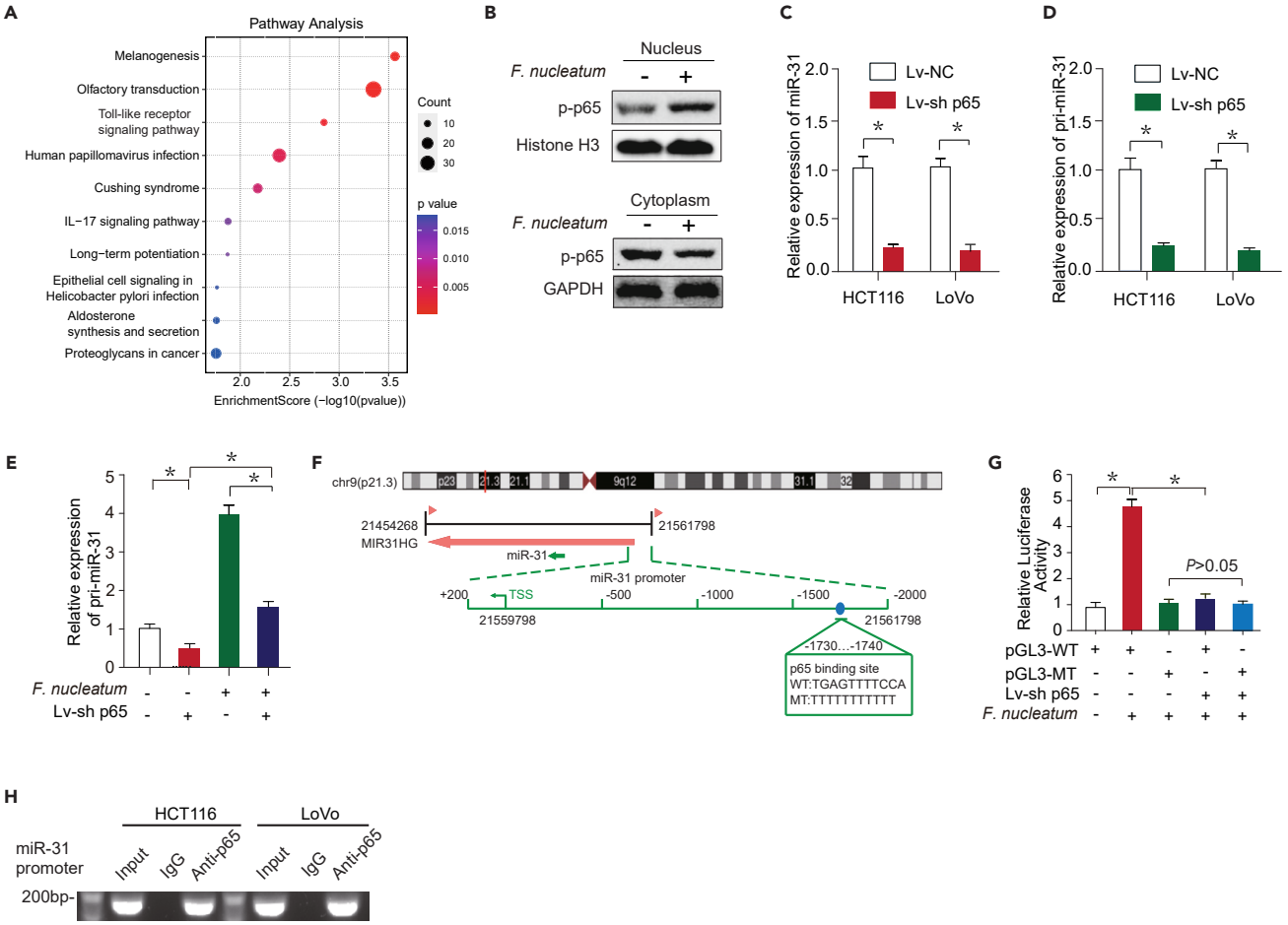

Figure 8. NF-κB is a transcription factor for miR-31

A) KEGG pathway analysis of a total of 1074 mRNAs involved in *F. nucleatum*-associated CRC.

(B) Western blotting was performed to measure the protein levels of phosphorylated p65 in the cytoplasm and nucleus of HCT116 cells after *F. nucleatum* infection.

(C and D) miR-31 and pri-miR-31 expression were detected by RT-qPCR in HCT116 or LoVo cells transfected with Lv-sh p65.

(E) HCT116 cells transfected with Lv-sh p65 were infected with *F. nucleatum* for 2 h, and the primary transcript (pri-miRNA) of miR-31 was quantified by real-time PCR. *p < 0.05.

(F) pGL3 luciferase reporter plasmids that either have the wild-type (WT) or mutant (MT) p65 binding site in the miR-31 promoter.

(G) Luciferase constructs (pGL3-WT or pGL3-MT) or Lv-sh p65 were co-transfected into HEK293T cells prior to *F. nucleatum* infection. The activity of luciferase was adjusted to match that of Renilla luciferase. *p < 0.05. (H) miR-31 promoter was detected in the chromatin sample immunoprecipitated from HCT116 (left) and LoVo (right) cells using an antibody against p65.

A schematic representation of the mechanism by which *F. nucleatum* induces intestinal inflammation and colorectal tumorigenesis via targeting NF-κB, miR-31, STX12, and the autophagy pathway.

nucleus, while it was downregulated in the cytoplasm (Figure 8B), suggesting that *F. nucleatum* stimulated an inflammatory response through activating NF-κB. To further understand the possible role of *F. nucleatum* in the regulation of miR-31 during CRC development, we utilized the JASPAR database (http://jaspar.genereg.net) to decipher potential transcription factors in the upstream of the transcription start site of miR-31. The consensus binding sequence (5′TGAGTTTTCCA-3′) for p65 (a subunit of NF-κB) was identified in the promoter region of miR-31. In HCT116 and LoVo cells, we knocked down p65 to test the hypothesis that p65 can bind to this area and control the expression of miR-31. We found that both miR-31 and pri-miR-31 expression were significantly downregulated by Lv-sh p65 (Figures 8C and 8D). Moreover, p65 regulated the relative expression of pri-miR-31 in HCT116 cells infected with *F. nucleatum* (Figure 8E). Next, luciferase reporter plasmids containing either WT (pGL3-WT) or MT p65 binding sites (pGL3-MT) were constructed in the miR-31 promoter region (Figure 8F). p65 short hairpin RNA significantly suppressed the luciferase activity of cells transfected with pGL3-WT during *F. nucleatum* infection but without inhibitory effects in cells transfected with pGL3-MT

(Figure 8G). Consistently, the ChIP assay showed that the miR-31 promoter region was significantly enriched by anti-p65, but not by its isotype IgG control in HCT116 and LoVo cells (Figure 8H). Together, these results show that *F. nucleatum* induces miR-31 expression through NF-κB.

DISCUSSION

This study found that *F. nucleatum* inhibited autophagic flux and induced miR-31 expression in CRC tissues and cells. MiR-31 expression was closely associated with the depth of invasion and tumor TNM stage and potentially associated with CRC formation and progression. MiR-31 blocked autophagic flux to benefit the intracellular survival of *F. nucleatum* by targeting STX12, which in turn led to the high expression of miR-31 in intestinal epithelial cells. Moreover, miR-31 promoted the proliferation of CRC cells by targeting eIF4EBP1 and eIF4EBP2, forming a positive feedback. These results showed the pathologic and tumorigenic roles of miR-31 in persistent *F. nucleatum* infection-induced CRC.

Previous studies have shown that miRNAs such as miR-21,[31] miR-34a,[36] and miR-124[37] can help bacteria communicate with their host and trigger the development of cancer by increasing cell proliferation and controlling key proteins.[37,38] The expression of miRNAs may be regulated by *F. nucleatum* infection during the development of CRC.[31,39,40] According to the results of the current study, miR-31, a downstream target of *F. nucleatum* in the colorectum, is crucial for the development and progression of CRCs during *F. nucleatum* infection. Our findings demonstrated that *F. nucleatum* and miR-31 expression are significantly abundant in CRC tissues, especially in more advanced cancers. Furthermore, miR-31 expression was positively associated with the *F. nucleatum* abundance in CRC tissues, and patients with a high miR-31 expression had worse clinical outcomes. In the present study, 56.9% (62/109) and 65.1% (71/109) of patients with CRC had high expression of miR-31 and *F. nucleatum* infection, respectively, which were significantly higher than the rates (23.1% and 24.3%, respectively) in patients without CRC, as previously reported,[41–44] indicating that both the high expression of miR-31 and *F. nucleatum* infection are associated with CRC. Several studies have reported that miR-31 enhances the tumor development and progression of some cancers such as pancreatic, cervical, and colorectal cancers but inhibits the tumorigenesis of other cancers such as ovarian and prostate cancers.[39,45–49] miR-31 in diverse tumor types exerts a dual contradictory functional role according to spatiotemporal specificity, which results from the pathological type and target genes in human cancers.[50]

Autophagy, which is responsible for capturing and digesting intracellular microorganisms, is a crucial participant in host innate immunity. A variety of microorganisms can escape immune response by inhibiting various stages of autophagy.[51,52] *F. nucleatum* is one of the few pathogens that can improve autophagosome generation during infection. *F. nucleatum* not only induces autophagosome formation to promote inflammatory responses in intestinal epithelial cells but also confers metastasis and chemoresistance by modulating autophagy in CRC and esophageal squamous cell carcinoma.[53,54] However, *F. nucleatum* also impairs autophagic flux to induce the production of pro-inflammatory cytokines *in vitro* and *in vivo*.[10,19,54] Consistent with these findings, this study found that *F. nucleatum* promoted autophagosome formation but inhibited autophagic flux. It is an interesting phenomenon that *F. nucleatum* increased both MAP1LC3B-I and MAP1LC3B-II expression in cells as shown in Figure 2F, whereas *F. nucleatum* increased the conversion of MAP1LC3B-I to MAP1LC3B-II, as shown in Figure 3H. Moreover, *F. nucleatum* infection further promoted the conversion of MAP1LC3B-I to MAP1LC3B-II in HCT116 cells transfected with miR-31 mimics, whereas *F. nucleatum* infection did not promote the conversion in HCT116 cells transfected with an miR-31 inhibitor as shown in Figure 3H, indicating that miR-31 plays a role in promoting the conversion of MAP1LC3B-I to MAP1LC3B-II. We postulate that *F. nucleatum* infection not only directly induces the expression of LC3B, including expression of MAP1LC3B-I and MAP1LC3B-II but also promotes the conversion of MAP1LC3B-I to MAP1LC3B-II, which is further enhanced by transfection with miR-31 mimics in HCT116 cells. It is most likely that miR-31 inhibits autophagic flux by inhibiting STX12, thus promoting the accumulation of MAP1LC3B-II and exhaustion of MAP1LC3B-I in HCT116 cells with *F. nucleatum* infection. Moreover, this study demonstrated that miR-31 enhanced these effects by inhibiting STX12, which resulted in the inhibition of the progression of autophagosome-lysosome fusion, and consequently the persistence of *F. nucleatum*-persistent infection inside the CRC cells and CRC tumorigenicity. In general, these findings indicate that *F. nucleatum* promotes autophagosome formation but impairs autophagic flux, which plays a pathogenic role in colorectal carcinogenesis.

STX12 is a member of the SNARE family localized to the endosome or autophagosome involved in the fusion between autophagosomes and lysosomes.[55,56] SNARE proteins are required for a series of membrane fusion events in the autophagy pathway, for example, vesicle-associated membrane protein 7

(VAMP7), VAMP8, Vti1b, and STX17 are required for the fusion between autophagosomes and endosomes/lysosomes,[57,58] which is considered the classic mechanism by which the SNARE protein is available to the completed autophagosome. In this study, STX12 was identified to be closely related to this fusion process, which we believe is a unique mechanism underlying the persistence of *F. nucleatum* infection. Knockdown of miR-31 reversed the downregulation of STX12 induced by *F. nucleatum in vitro* and *in vivo*, and STX12 silencing resulted in significantly increased intracellular survival of *F. nucleatum*. In addition, STX12 knockdown significantly increased the conversion of LC3-I to LC3-II and simultaneously increased SQSTM1 protein expression. These findings indicate that miR-31 inhibits autophagic flux-mediated elimination of intracellular *F. nucleatum* by targeting STX12, which provides a new 'SNARE complex' theory and a new mode for a pathogen to escape the host immune response.

This study showed that *F. nucleatum*-induced miR-31 expression inhibited the expression of eIF4EBP1/2, leading to the proliferation of CRC cells. eIF4EBP1 and eIF4EBP2 belong to the 4E-binding protein family, which includes eIF4EBP1, eIF4EBP2, and eIF4EBP3, and negatively regulates the assembly of eIF4F from its components by inhibiting the interaction of eIF4E with eIF4G.[59] eIF4E and eIF4G are important components of eIF4F complex, which regulates the initiation of cap-dependent mRNA translation.[60] Therefore, inhibition of eIF4EBP1/2 promotes translation. Additionally, eIF4EBP1/2 overexpression has been seen in prostate, head and neck, and breast cancers and is linked to a poor prognosis.[61,62] In this study, *F. nucleatum* reduced the expression of eIF4EBP1/2, which was reversed by miR-31 knockdown, and overexpression of miR-31 further reduced the expression of eIF4EBP1/2 *in vitro* and *in vivo*. Furthermore, inhibition of eIF4EBP1/2 through miR-31 promoted CRC cell proliferation, and knockdown of eIF4EBP1/2 inhibited inflammation and increased the colonization of *F. nucleatum* in the colorectal tissues of miR-31 ^{wt} and miR-31$^{-/-}$ mice. These findings indicate that *F. nucleatum* can reduce the expression of eIF4EBP1/2 by inducing miR-31, and eIF4EBP1/2 acts as a growth suppressor of CRC. Although the complex relationship between the tumor-suppressive and oncogenic functions of eIF4EBP1/2 is not fully understood, *F. nucleatum*/miR-31/eIF4EBP1/2 pathway may, at least in part, explain how *F. nucleatum* infection promotes cell proliferation in CRC.

In conclusion, *F. nucleatum* inhibits autophagic flux by inducing miR-31, which directly targets STX12, leading to persistent *F. nucleatum* infection in CRC. Moreover, miRNA-31 modulates cell proliferation in CRC by directly targeting eIF4EBP1/2. These findings provide novel insights into the pathogenic role of *F. nucleatum* in CRC and open new avenues for targeting autophagy as well as miRNA alterations for CRC prevention and treatment.

Limitations of the study

Based on the findings of this study, we propose that *F. nucleatum* inhibits autophagic flux and promotes CRC tumorigenesis through the miR-31/STX12/eIF4EBP1/2 pathway. Further extensive investigation is needed to confirm the findings, especially the interrelationships among miR-31, STX12, and eIF4EBP1/2 and their upstream regulators and downstream targets as well their precise roles. In addition, the persistence of bacterial infection leads to chronic inflammation, and *F. nucleatum*-elicited inflammation plays an important role in the tumorigenesis of CRC. Conversely, CRC cannot be caused by inflammation without the ongoing presence of bacteria or compounds derived from bacteria.[63] Therefore, greater efforts should be made to comprehend the inflammation that *F. nucleatum* causes as well as how to cease the persistent *F. nucleatum* infection. Currently, our team is conducting bacterial gene manipulation on *F. nucleatum* to explore the role and mechanism of its genes in inflammation and tumorigenesis of CRC induced by *F. nucleatum*.

STAR★METHODS

Detailed methods are provided in the online version of this paper and include the following:

- KEY RESOURCES TABLE
- RESOURCE AVAILABILITY
  - Lead contact
  - Materials availability
  - Data and code availability
- EXPERIMENTAL MODEL AND SUBJECT DETAILS
  - Human subjects and tissues
  - Animal experiments
  - Bacterial strains and cell lines

SUPPLEMENTAL INFORMATION

Supplemental information can be found online at https://doi.org/10.1016/j.isci.2023.106770.

ACKNOWLEDGMENTS

The authors would like to thank patients with colorectal cancer who donated their specimen and time to this study. This work was supported by grants from the National Natural Science Foundation of China (no. 81501796 and 82102744), Natural Science Foundation of Chongqing (no. cstc2017jcyjAX0205 and cstc2020jcyj-msxmX0220), the project of school management in Army Medical University (no. 31024629). The authors thank Medjaden Inc. for its assistance in the preparation of the manuscript.

AUTHOR CONTRIBUTIONS

Conceptualization, X.H.M., D.Z.Z., and Q.L.; Methodology, B.T., X.X.L., Y.N.T., Y.Y.F., Y.L.M., G.D.D., and J.L.; Formal Analysis, Q.L.X., T.Z., and J.Z.; Visualization, L.D., X.Y.H., Y.Z.L., H.X.L., L.H.Z., and Y.Y.X.; Writing – Original Draft, B.T. and X.X.L.; Writing – Review & Editing, B.T. and X.H.M.; Supervision, X.H.M., Q.L., and D.Z.Z.; Funding Acquisition, B.T. and Q.L.

DECLARATION OF INTERESTS

The authors declare that they have no conflict of interest.

Received: December 23, 2022
Revised: February 27, 2023
Accepted: April 24, 2023
Published: April 26, 2023

REFERENCES

1. Engevik, M.A., Danhof, H.A., Auchtung, J., Endres, B.T., Ruan, W., Bassères, E., Engevik, A.C., Wu, Q., Nicholson, M., Luna, R.A., et al. (2021). Fusobacterium nucleatum adheres to clostridioides difficile via the RadD adhesin to enhance biofilm formation in intestinal mucus. Gastroenterology *160*, 1301–1314.e8. https://doi.org/10.1053/j.gastro.2020.11.034.

2. Han, Y.W. (2015). Fusobacterium nucleatum: a commensal-turned pathogen. Curr. Opin. Microbiol. *23*, 141–147. https://doi.org/10.1016/j.mib.2014.11.013.

3. Bashir, A., Miskeen, A.Y., Hazari, Y.M., Asrafuzzaman, S., and Fazili, K.M. (2016). Fusobacterium nucleatum, inflammation, and immunity: the fire within human gut. Tumour Biol. *37*, 2805–2810. https://doi.org/10.1007/s13277-015-4724-0.

4. Brennan, C.A., and Garrett, W.S. (2019). Fusobacterium nucleatum-symbiont, opportunist and oncobacterium. Nat. Rev. Microbiol. *17*, 156–166. https://doi.org/10.1038/s41579-018-0129-6.

5. Komiya, Y., Shimomura, Y., Higurashi, T., Sugi, Y., Arimoto, J., Umezawa, S., Uchiyama, S., Matsumoto, M., and Nakajima, A. (2019). Patients with colorectal cancer have identical strains of Fusobacterium nucleatum in their colorectal cancer and oral cavity. Gut *68*, 1335–1337. https://doi.org/10.1136/gutjnl-2018-316661.

6. Castellarin, M., Warren, R.L., Freeman, J.D., Dreolini, L., Krzywinski, M., Strauss, J., Barnes, R., Watson, P., Allen-Vercoe, E., Moore, R.A., and Holt, R.A. (2012). Fusobacterium nucleatum infection is prevalent in human colorectal carcinoma. Genome Res. *22*, 299–306. https://doi.org/10.1101/gr.126516.111.

7. Kostic, A.D., Gevers, D., Pedamallu, C.S., Michaud, M., Duke, F., Earl, A.M., Ojesina, A.I., Jung, J., Bass, A.J., Tabernero, J., et al.

(2012). Genomic analysis identifies association of Fusobacterium with colorectal carcinoma. Genome Res. *22*, 292–298. https://doi.org/10.1101/gr.126573.111.

8. Kostic, A.D., Chun, E., Robertson, L., Glickman, J.N., Gallini, C.A., Michaud, M., Clancy, T.E., Chung, D.C., Lochhead, P., Hold, G.L., et al. (2013). Fusobacterium nucleatum potentiates intestinal tumorigenesis and modulates the tumor-immune microenvironment. Cell Host Microbe *14*, 207–215. https://doi.org/10.1016/j.chom.2013.07.007.

9. Chen, Y., Chen, Y., Zhang, J., Cao, P., Su, W., Deng, Y., Zhan, N., Fu, X., Huang, Y., and Dong, W. (2020). Fusobacterium nucleatum promotes metastasis in colorectal cancer by activating autophagy signaling via the upregulation of CARD3 expression. Theranostics *10*, 323–339. https://doi.org/10.7150/thno.38870.

10. Tang, B., Wang, K., Jia, Y.P., Zhu, P., Fang, Y., Zhang, Z.J., Mao, X.H., Li, Q., and Zeng, D.Z. (2016). Fusobacterium nucleatum-induced impairment of autophagic flux enhances the expression of proinflammatory cytokines via ROS in caco-2 cells. PLoS One *11*, e0165701. https://doi.org/10.1371/journal.pone.0165701.

11. Yu, T., Guo, F., Yu, Y., Sun, T., Ma, D., Han, J., Qian, Y., Kryczek, I., Sun, D., Nagarsheth, N., et al. (2017). Fusobacterium nucleatum promotes chemoresistance to colorectal cancer by modulating autophagy. Cell *170*, 548–563.e16. https://doi.org/10.1016/j.cell.2017.07.008.

12. Gursoy, U.K., Könönen, E., and Uitto, V.J. (2008). Intracellular replication of fusobacteria requires new actin filament formation of epithelial cells. APMIS *116*, 1063–1070. https://doi.org/10.1111/j.1600-0463.2008.00868.x.

13. Haruki, K., Kosumi, K., Hamada, T., Twombly, T.S., Väyrynen, J.P., Kim, S.A., Masugi, Y., Qian, Z.R., Mima, K., Baba, Y., et al. (2020). Association of autophagy status with amount of Fusobacterium nucleatum in colorectal cancer. J. Pathol. *250*, 397–408. https://doi.org/10.1002/path.5381.

14. Lee, P., and Tan, K.S. (2014). Fusobacterium nucleatum activates the immune response through retinoic acid-inducible gene I. J. Dent. Res. *93*, 162–168. https://doi.org/10.1177/0022034513516346.

15. Liu, H., Hong, X.L., Sun, T.T., Huang, X.W., Wang, J.L., and Xiong, H. (2020). Fusobacterium nucleatum exacerbates colitis by damaging epithelial barriers and inducing aberrant inflammation. J. Dig. Dis. *21*, 385–398. https://doi.org/10.1111/1751-2980.12909.

16. Amano, A., Nakagawa, I., and Yoshimori, T. (2006). Autophagy in innate immunity against intracellular bacteria. J. Biochem. *140*, 161–166. https://doi.org/10.1093/jb/mvj162.

17. Klionsky, D.J., Abdel-Aziz, A.K., Abdelfatah, S., Abdellatif, M., Abdoli, A., Abel, S., Abeliovich, H., Abildgaard, M.H., Abudu, Y.P., Acevedo-Arozena, A., et al. (2021). Guidelines for the use and interpretation of assays for monitoring autophagy (4th edition). Autophagy *17*, 1–382. https://doi.org/10.1080/15548627.2020.1797280.

18. Wu, Y., Yao, J., Xie, J., Liu, Z., Zhou, Y., Pan, H., and Han, W. (2018). The role of autophagy in colitis-associated colorectal cancer. Signal Transduct. Target. Ther. *3*, 31. https://doi.org/10.1038/s41392-018-0031-8.

19. Duan, C., Tang, X., Wang, W., Qian, W., Fu, X., Deng, X., Zhou, S., Han, C., and Hou, X. (2021). Lactobacillus rhamnosus attenuates intestinal inflammation induced by Fusobacterium nucleatum infection by restoring the autophagic flux. Int. J. Mol. Med. *47*, 125–136. https://doi.org/10.3892/ijmm.2020.4780.

20. Komoll, R.M., Hu, Q., Olarewaju, O., von Döhlen, L., Yuan, Q., Xie, Y., Tsay, H.C., Daon, J., Qin, R., Manns, M.P., et al. (2021). MicroRNA-342-3p is a potent tumour suppressor in hepatocellular carcinoma. J. Hepatol. *74*, 122–134. https://doi.org/10.1016/j.jhep.2020.07.039.

21. Shibuya, N., Kakeji, Y., and Shimono, Y. (2020). MicroRNA-93 targets WASF3 and functions as a metastasis suppressor in breast cancer. Cancer Sci. *111*, 2093–2103. https://doi.org/10.1111/cas.14423.

22. Wang, C., Tian, S., Zhang, D., Deng, J., Cai, H., Shi, C., and Yang, W. (2020). Increased expression of microRNA-93 correlates with progression and prognosis of prostate cancer. Medicine (Baltim.) *99*, e18432. https://doi.org/10.1097/MD.0000000000018432.

23. Aguilar, C., Mano, M., and Eulalio, A. (2019). MicroRNAs at the host-bacteria interface: host defense or bacterial offense. Trends Microbiol. *27*, 206–218. https://doi.org/10.1016/j.tim.2018.10.011.

24. De Martinis, M., Ginaldi, L., Allegra, A., Sirufo, M.M., Pioggia, G., Tonacci, A., and Gangemi, S. (2020). The osteoporosis/microbiota linkage: the role of miRNA. Int. J. Mol. Sci. *21*, 8887. https://doi.org/10.3390/ijms21238887.

25. Kumar, M., Sahu, S.K., Kumar, R., Subuddhi, A., Maji, R.K., Jana, K., Gupta, P., Raffetseder, J., Lerm, M., Ghosh, Z., et al. (2015). MicroRNA let-7 modulates the immune response to Mycobacterium tuberculosis infection via control of A20, an inhibitor of the NF-κB pathway. Cell Host Microbe *17*, 345–356. https://doi.org/10.1016/j.chom.2015.01.007.

26. Li, Q., Fang, Y., Zhu, P., Ren, C.Y., Chen, H., Gu, J., Jia, Y.P., Wang, K., Tong, W.D., Zhang, W.J., et al. (2015). Burkholderia pseudomallei survival in lung epithelial cells benefits from miRNA-mediated suppression of ATG10. Autophagy *11*, 1293–1307. https://doi.org/10.1080/15548627.2015.1058474.

27. Tang, B., Li, N., Gu, J., Zhuang, Y., Li, Q., Wang, H.G., Fang, Y., Yu, B., Zhang, J.Y., Xie, Q.H., et al. (2012). Compromised autophagy by MIR30B benefits the intracellular survival of Helicobacter pylori. Autophagy *8*, 1045–1057. https://doi.org/10.4161/auto.20159.

28. Lv, D., Xiang, Y., Yang, Q., Yao, J., and Dong, Q. (2020). Long non-coding RNA TUG1 promotes cell proliferation and inhibits cell apoptosis, autophagy in clear cell renal cell carcinoma via MiR-31-5p/FLOT1 Axis. OncoTargets Ther. *13*, 5857–5868. https://doi.org/10.2147/OTT.S254634.

29. Yang, X., Xu, X., Zhu, J., Zhang, S., Wu, Y., Wu, Y., Zhao, K., Xing, C., Cao, J., Zhu, H., et al. (2016). miR-31 affects colorectal cancer cells by inhibiting autophagy in cancer-associated fibroblasts. Oncotarget *7*, 79617–79628. https://doi.org/10.18632/oncotarget.12873.

30. Feng, Y.Y., Zeng, D.Z., Tong, Y.N., Lu, X.X., Dun, G.D., Tang, B., Zhang, Z.J., Ye, X.L., Li, Q., Xie, J.P., and Mao, X.H. (2019). Alteration of microRNA-4474/4717 expression and CREB-binding protein in human colorectal cancer tissues infected with Fusobacterium nucleatum. PLoS One *14*, e0215088. https://doi.org/10.1371/journal.pone.0215088.

31. Yang, Y., Weng, W., Peng, J., Hong, L., Yang, L., Toiyama, Y., Gao, R., Liu, M., Yin, M., Pan, C., et al. (2017). Fusobacterium nucleatum increases proliferation of colorectal cancer cells and tumor development in mice by activating toll-like receptor 4 signaling to nuclear factor-κb, and up-regulating expression of MicroRNA-21. Gastroenterology *152*, 851–866.e24. https://doi.org/10.1053/j.gastro.2016.11.018.

32. Koike, S., and Jahn, R. (2019). SNAREs define targeting specificity of trafficking vesicles by combinatorial interaction with tethering factors. Nat. Commun. *10*, 1608. https://doi.org/10.1038/s41467-019-09617-9.

33. Cai, W., Ye, Q., and She, Q.B. (2014). Loss of 4E-BP1 function induces EMT and promotes cancer cell migration and invasion via cap-dependent translational activation of snail. Oncotarget *5*, 6015–6027. https://doi.org/10.18632/oncotarget.2109.

34. Petroulakis, E., Parsyan, A., Dowling, R.J.O., LeBacquer, O., Martineau, Y., Bidinosti, M., Larsson, O., Alain, T., Rong, L., Mamane, Y., et al. (2009). p53-dependent translational control of senescence and transformation via 4E-BPs. Cancer Cell *16*, 439–446. https://doi.org/10.1016/j.ccr.2009.09.025.

35. Hoesel, B., and Schmid, J.A. (2013). The complexity of NF-κB signaling in inflammation and cancer. Mol. Cancer *12*, 86. https://doi.org/10.1186/1476-4598-12-86.

36. Li, H., Rokavec, M., Jiang, L., Horst, D., and Hermeking, H. (2017). Antagonistic effects of p53 and HIF1A on microRNA-34a regulation of PPP1R11 and STAT3 and hypoxia-induced epithelial to mesenchymal transition in colorectal cancer cells. Gastroenterology *153*, 505–520. https://doi.org/10.1053/j.gastro.2017.04.017.

37. Qiu, Z., Guo, W., Wang, Q., Chen, Z., Huang, S., Zhao, F., Yao, M., Zhao, Y., and He, X. (2015). MicroRNA-124 reduces the pentose phosphate pathway and proliferation by targeting PRPS1 and RPIA mRNAs in human colorectal cancer cells. Gastroenterology *149*, 1587–1598.e11. https://doi.org/10.1053/j.gastro.2015.07.050.

38. Proença, M.A., Biselli, J.M., Succi, M., Severino, F.E., Berardinelli, G.N., Caetano, A., Reis, R.M., Hughes, D.J., and Silva, A.E. (2018). Relationship between Fusobacterium nucleatum, inflammatory mediators and microRNAs in colorectal carcinogenesis. World J. Gastroenterol. *24*, 5351–5365. https://doi.org/10.3748/wjg.v24.i47.5351.

39. Davenport, M.L., Echols, J.B., Silva, A.D., Anderson, J.C., Owens, P., Yates, C., Wei, Q., Harada, S., Hurst, D.R., and Edmonds, M.D. (2021). miR-31 displays subtype specificity in lung cancer. Cancer Res. *81*, 1942–1953. https://doi.org/10.1158/0008-5472.CAN-20-2769.

40. Zhao, Y., Tao, Q., Li, S., Zheng, P., Liu, J., and Liang, X. (2020). Both endogenous and exogenous miR-139-5p inhibit Fusobacterium nucleatum-related colorectal cancer development. Eur. J. Pharmacol. *888*, 173459. https://doi.org/10.1016/j.ejphar.2020.173459.

41. Eklöf, V., Löfgren-Burström, A., Zingmark, C., Edin, S., Larsson, P., Karling, P., Alexeyev, O., Rutegård, J., Wikberg, M.L., and Palmqvist, R. (2017). Cancer-associated fecal microbial markers in colorectal cancer detection. Int. J. Cancer *141*, 2528–2536. https://doi.org/10.1002/ijc.31011.

42. Yachida, S., Mizutani, S., Shiroma, H., Shiba, S., Nakajima, T., Sakamoto, T., Watanabe, H., Masuda, K., Nishimoto, Y., Kubo, M., et al. (2019). Metagenomic and metabolomic analyses reveal distinct stage-specific phenotypes of the gut microbiota in colorectal cancer. Nat. Med. *25*, 968–976. https://doi.org/10.1038/s41591-019-0458-7.

43. Nosho, K., Igarashi, H., Nojima, M., Ito, M., Maruyama, R., Yoshii, S., Naito, T., Sukawa, Y., Mikami, M., Sumioka, W., et al. (2014). Association of microRNA-31 with BRAF mutation, colorectal cancer survival and serrated pathway. Carcinogenesis *35*, 776–783. https://doi.org/10.1093/carcin/bgt374.

44. Zhou, P., Yang, D., Sun, D., and Zhou, Y. (2022). Gut microbiome: new biomarkers in early screening of colorectal cancer. J. Clin. Lab. Anal. *36*, e24359. https://doi.org/10.1002/jcla.24359.

45. Braga, E.A., Fridman, M.V., and Kushlinskii, N.E. (2017). Molecular mechanisms of ovarian carcinoma metastasis: key genes and regulatory MicroRNAs. Biochemistry *82*, 529–541. https://doi.org/10.1134/S0006297917050017.

46. Hsu, H.H., Kuo, W.W., Shih, H.N., Cheng, S.F., Yang, C.K., Chen, M.C., Tu, C.C., Viswanadha, V.P., Liao, P.H., and Huang, C.Y. (2019). FOXC1 regulation of miR-31-5p confers oxaliplatin resistance by targeting LATS2 in colorectal cancer. Cancers *11*, 1576. https://doi.org/10.3390/cancers11101576.

47. Izquierdo, L., Montalbo, R., Ingelmo-Torres, M., Mallofré, C., Ramírez-Backhaus, M., Rubio, J., Van der Heijden, A.G., Schaafsma, E., Lopez-Beltran, A., Blanca, A., et al. (2017). Prognostic microRNAs in upper tract urothelial carcinoma: multicenter and international validation study. Oncotarget *8*, 51522–51529. https://doi.org/10.18632/oncotarget.17884.

48. Lai, Y.H., Liu, H., Chiang, W.F., Chen, T.W., Chu, L.J., Yu, J.S., Chen, S.J., Chen, H.C., and Tan, B.C.M. (2018). MiR-31-5p-ACOX1 Axis enhances tumorigenic fitness in oral squamous cell carcinoma via the promigratory prostaglandin E2. Theranostics *8*, 486–504. https://doi.org/10.7150/thno.22059.

49. Wang, N., Li, Y., and Zhou, J. (2017). miR-31 functions as an oncomir which promotes epithelial-mesenchymal transition via regulating BAP1 in cervical cancer. BioMed Res. Int. *2017*, 6361420. https://doi.org/10.1155/2017/6361420.

50. Loya, C.M., Lu, C.S., Van Vactor, D., and Fulga, T.A. (2009). Transgenic microRNA inhibition with spatiotemporal specificity in intact organisms. Nat. Methods *6*, 897–903. https://doi.org/10.1038/nmeth.1402.

51. Choy, A., Dancourt, J., Mugo, B., O'Connor, T.J., Isberg, R.R., Melia, T.J., and Roy, C.R. (2012). The Legionella effector RavZ inhibits host autophagy through irreversible Atg8 deconjugation. Science *338*, 1072–1076. https://doi.org/10.1126/science.1227026.

52. Kayath, C.A., Hussey, S., El hajjami, N., Nagra, K., Philpott, D., and Allaoui, A. (2010). Escape of intracellular Shigella from autophagy requires binding to cholesterol through the type III effector, IcsB. Microb. Infect. *12*, 956–966. https://doi.org/10.1016/j.micinf.2010.06.006.

53. Liu, Y., Baba, Y., Ishimoto, T., Tsutsuki, H., Zhang, T., Nomoto, D., Okadome, K., Yamamura, K., Harada, K., Eto, K., et al. (2021). Fusobacterium nucleatum confers chemoresistance by modulating autophagy in oesophageal squamous cell carcinoma. Br. J. Cancer *124*, 963–974. https://doi.org/10.1038/s41416-020-01198-5.

54. Su, W., Chen, Y., Cao, P., Chen, Y., Guo, Y., Wang, S., and Dong, W. (2020). Fusobacterium nucleatum promotes the development of ulcerative colitis by inducing the autophagic cell death of intestinal epithelial. Front. Cell. Infect. Microbiol. *10*, 594806. https://doi.org/10.3389/fcimb.2020.594806.

55. Lu, Y., Zhang, Z., Sun, D., Sweeney, S.T., and Gao, F.B. (2013). Syntaxin 13, a genetic modifier of mutant CHMP2B in frontotemporal dementia, is required for autophagosome maturation. Mol. Cell *52*, 264–271. https://doi.org/10.1016/j.molcel.2013.08.041.

56. Tang, B.L., Tan, A.E., Lim, L.K., Lee, S.S., Low, D.Y., and Hong, W. (1998). Syntaxin 12, a member of the syntaxin family localized to the endosome. J. Biol. Chem. *273*, 6944–6950. https://doi.org/10.1074/jbc.273.12.6944.

57. Furuta, N., Fujita, N., Noda, T., Yoshimori, T., and Amano, A. (2010). Combinational soluble N-ethylmaleimide-sensitive factor attachment protein receptor proteins VAMP8 and Vti1b mediate fusion of antimicrobial and canonical autophagosomes with lysosomes. Mol. Biol. Cell *21*, 1001–1010. https://doi.org/10.1091/mbc.e09-08-0693.

58. Itakura, E., Kishi-Itakura, C., and Mizushima, N. (2012). The hairpin-type tail-anchored SNARE syntaxin 17 targets to autophagosomes for fusion with endosomes/lysosomes. Cell *151*, 1256–1269. https://doi.org/10.1016/j.cell.2012.11.001.

59. Musa, J., Orth, M.F., Dallmayer, M., Baldauf, M., Pardo, C., Rotblat, B., Kirchner, T., Leprivier, G., and Grünewald, T.G.P. (2016). Eukaryotic initiation factor 4E-binding protein 1 (4E-BP1): a master regulator of mRNA translation involved in tumorigenesis. Oncogene *35*, 4675–4688. https://doi.org/10.1038/onc.2015.515.

60. Siddiqui, N., Tempel, W., Nedyalkova, L., Volpon, L., Wernimont, A.K., Osborne, M.J., Park, H.W., and Borden, K.L.B. (2012). Structural insights into the allosteric effects of 4EBP1 on the eukaryotic translation initiation factor eIF4E. J. Mol. Biol. *415*, 781–792. https://doi.org/10.1016/j.jmb.2011.12.002.

61. Qin, X., Jiang, B., and Zhang, Y. (2016). 4E-BP1, a multifactor regulated multifunctional protein. Cell Cycle *15*, 781–786. https://doi.org/10.1080/15384101.2016.1151581.

62. Wang, R., Ganesan, S., and Zheng, X.F.S. (2016). Yin and yang of 4E-BP1 in cancer. Cell Cycle *15*, 1401–1402. https://doi.org/10.1080/15384101.2016.1168200.

63. Arthur, J.C., Perez-Chanona, E., Mühlbauer, M., Tomkovich, S., Uronis, J.M., Fan, T.J., Campbell, B.J., Abujamel, T., Dogan, B., Rogers, A.B., et al. (2012). Intestinal inflammation targets cancer-inducing activity of the microbiota. Science *338*, 120–123. https://doi.org/10.1126/science.1224820.

64. Lu, X., Xu, Q., Tong, Y., Zhang, Z., Dun, G., Feng, Y., Tang, J., Han, D., Mao, Y., Deng, L., et al. (2022). Long non-coding RNA EVADR induced by Fusobacterium nucleatum infection promotes colorectal cancer metastasis. Cell Rep. *40*, 111127. https://doi.org/10.1016/j.celrep.2022.111127.

65. Xu, Q., Lu, X., Li, J., Feng, Y., Tang, J., Zhang, T., Mao, Y., Lan, Y., Luo, H., Zeng, L., et al. (2022). Fusobacterium nucleatum induces excess methyltransferase-like 3-mediated microRNA-4717-3p maturation to promote colorectal cancer cell proliferation. Cancer Sci. *113*, 3787–3800. https://doi.org/10.1111/cas.15536.

66. Wirths, O. (2017). Extraction of soluble and insoluble protein fractions from mouse brains and spinal cords. Bio. Protoc. *7*, e2422. https://doi.org/10.21769/BioProtoc.2422.

STAR★METHODS

KEY RESOURCES TABLE

REAGENT or RESOURCE	SOURCE	IDENTIFIER
Antibodies		
Anti-STX12	Sigma	Cat# SAB1400469, RRID:AB_1857621
Anti-MAP1LC3B-I/II	Sigma	Cat# L7543;RRID:AB_796155
Anti-Phospho-NF-κB p65	Cell Signaling	Cat# 3033, RRID:AB_331284
Anti-GAPDH	Cell Signaling	Cat# 5174, RRID:AB_10622025
Anti-SQSTM1	Cell Signaling	Cat# 5114, RRID:AB_10624872
Anti-Rabbit IgG	Cell Signaling	Cat# 7074, RRID:AB_2099233
Anti-Mouse IgG	Cell Signaling	Cat# 7076, RRID:AB_330924
Anti-eIF4EBP1	Cell Signaling	Cat# 9644, RRID:AB_2097841
Anti-eIF4EBP2	Cell Signaling	Cat# 2845, RRID:AB_10699019
Anti-p65	Cell Signaling	Cat# 8242, RRID:AB_10859369
Rabbit (DA1E) mAb IgG XP® Isotype Control	Cell Signaling	Cat# 3900, RRID:AB_1550038
Anti-Ki-67	Abcam	Cat# ab92742, RRID:AB_10562976
Goat Anti-Rabbit IgG H&L (HRP)	Abcam	Cat# ab97051, RRID:AB_10679369
Bacterial and virus strains		
F. nucleatum subsp. nucleatum	ATCC	ATCC 25586
Escherichia coli DH5α	Invitrogen	Cat# 18288019
pMIR-REPORT^{TM} luciferase vector	Promega	Cat# E1330
pGL3 Basic Vector	Promega	Cat# E1751
pSLenti-EF1a-EGFP-F2A vector	OBiO Co.	N/A
pLKD-CMV-EGFP-2A vector	OBiO Co.	N/A
GFP-LC3 plasmid	Addgene	RRID:Addgene_22405
mRFP-GFP-LC3 adenovirus	Hanheng Co.	N/A
p65 shRNA (human) lentivirus	Santa Cruz	Cat# sc-29410-V
STX12 shRNA (human) lentivirus	Santa Cruz	Cat# sc-88621-V
TUG1-pcDNA3.1 plasmid	Sangon Biotech	N/A
Biological samples		
Colonic tissue samples	the Third Hospital of CQMU and Southwest Hospital of AMU	N/A
Clinical information of CRC patients, see Tables S1 and S2	This paper	N/A
Chemicals, peptides, and recombinant proteins		
TRIzol	Invitrogen	Cat# 15596026
azoxymethane	Sigma	Cat# A5486
dextran sodium sulfate	MP Biomedicals	Cat# 0216011050
Fetal bovine serum	Gibco	Cat# 10100147
DAPI	Sigma	Cat# D9642
4% paraformaldehyde	Beyotime	Cat# P0099
3% BSA Albumin from bovine serum	biosharp	Cat# B0015k021000
PMSF	Beyotime	Cat# ST506
Harris hematoxylin	Solarbio	Cat# H8070
Eosin	Solarbio	Cat# G1100

(*Continued on next page*)

Continued

REAGENT or RESOURCE	SOURCE	IDENTIFIER
Triton X-100	Sigma-aldrich	Cat# SLBT3016
puromycin	Sigma	Cat# P8833
3,3′-diaminobenzidine	Sigma-Aldrich	Cat# D12384S
Anaerobic Basal Broth	Oxoid	Cat# 2215990
saponin	Sigma	Cat# S7900
Lipofectamine 3000	Invitrogen	Cat# L3000015
T-PER Tissue Protein Extraction Reagent	ThermoFisher	Cat# 78510
polyvinylidene fluoride membranes	Millipore	Cat# A29545253
5-ethynyl-20′-deoxyuridine	Beyotime	Cat# C0075
rapamycin	Sigma	Cat# S7418
RNase inhibitor	ThermoFisher	Cat# 87785
bicinchoninic acid (BCA) assay	Beyotime	Cat# P0010
3-methyladenine	Sigma	Cat# M9281
gentamicin	Sigma	Cat# G3632
metronidazole	Sigma	Cat# M1547
chloroquine	Sigma	Cat# C6628
Critical commercial assays		
QIAamp DNA Mini Kit	Qiagen	Cat# 51304
Premix EX Taq™ kit	Takara	Cat# RR390A
PrimeScript™ RT reagent Kit	Tarkara	Cat# RR047A
TB Green® Premix Ex Taq™	Tarkara	Cat# RR420A
Cell Counting Kit-8	Beyotime	Cat# C0038
TaqMan™ microRNA Reverse Transcription Kit	ABI	Cat# 4366596
TaqMan™ MicroRNA Assay Kit	ABI	Cat# 4427975
PrimeScript RT-PCR kits	Tarkara	Cat# DRR037
The T-PER™ Tissue Protein Extraction Reagent	Thermo	Cat# 78510
the ChIP Assay Kit	Beyotime	Cat# P2080S
Deposited data		
Transcriptome arrays of CRC tissues	This paper	GEO: GSE122182, GSE122183
Experimental models: Cell lines		
LoVo cells	ATCC	ATCC CCL-229,RRID:CVCL_0399
NCM460	OTWO, Shanghai	Cat# HTX1841,RRID:CVCL_0460
SW480	ATCC	ATCC CCL-228,RRID:CVCL_0546
SW620	ATCC	ATCC CCL-227,RRID:CVCL_0547
HT29	ATCC	ATCC HTB-38,RRID:CVCL_0320
HCT116	ATCC	ATCC CCL-247,RRID:CVCL_0291
HEK293	ATCC	Cat# CRL-1573, RRID:CVCL_0045
Experimental models: Organisms/strains		
BALB/c nude mice	Beijing Vital River	N/A
C57BL/6J wild-type (WT) mice	Beijing Vital River	N/A
C57BL/6J miR-31 knockout mice	Shanghai Paizhi Biotechnology Co.	N/A
Oligonucleotides		
miR-31 mimic	Thermo	Cat# 4464066
miR-31 inhibitor	Thermo	Cat# 4464084

(*Continued on next page*)

Continued

REAGENT or RESOURCE	SOURCE	IDENTIFIER
miR-31 control	Thermo	Cat# 4464058
siRNA eIF4EBP1	Sangon Biotech	N/A
siRNA eIF4EBP2	Sangon Biotech	N/A
DNA oligonucleotides of the luciferase report vectors, see Table S4	This paper	N/A
Primer for miR-31 promoter reporter, see Table S5	This paper	N/A
Primer for ChIP assay, see Table S6	This paper	N/A
Primers used in this study, see Table S3	This paper	N/A
Recombinant DNA		
pcDNA3.1-eIF4EBP1	Sangon Biotech	N/A
pcDNA3.1-eIF4EBP2	Sangon Biotech	N/A
pcDNA3.1-STX12	Sangon Biotech	N/A
Software and algorithms		
Zen 2012 software	Zeiss, Oberkochen	N/A
GraphPad Prism 6.0	GraphPad	RRID:SCR_002798
SPSS Statistics 20.0 software	IBM	RRID:SCR_016479
Other		
C1000TM Thermal Cycler	CFX96 Real-Time System	RRID:SCR_018064
Agilent 2100 Bioanalyzer	Agilent Technologies, Santa Clara	N/A
Bruker In-Vivo Xtreme II	Bruker BioSpin	N/A
Zeiss 800 laser scanning confocal microscope	Zeiss, Oberkochen	N/A

RESOURCE AVAILABILITY

Lead contact

Further information and requests for resources and reagents should be directed to and will be fulfilled by the lead contact, Xuhu Mao (maoxh2012@hotmail.com).

Materials availability

All materials generated in this study are available from the lead contact without restriction.

Data and code availability

- Raw data generated from transcriptome arrays of CRC tissues have been deposited in the Gene Expression Omnibus and are available under accession number GSE122182 and GSE122183.
- This paper does not report original code.
- Any additional information required to reanalyze the data reported in this paper is available from the lead contact upon request.

EXPERIMENTAL MODEL AND SUBJECT DETAILS

Human subjects and tissues

In this study, CRC tissues, paracancerous normal-appearing tissues from CRC patients or colorectal polyp tissues from patients were used to analyze the association between *F. nucleatum* infection and CRC, the effects of *F. nucleatum* on recurrence-free survival (RFS), and the potential involvement of miRNAs in *F. nucleatum*-induced CRC. The study protocol was approved by the Ethics Committee of the Third Affiliated Hospital to Chongqing Medical University (2018-17) and all participants signed informed consent forms. Clinical data for each patient information are presented in Table S1 and S2, regarding patient age, gender, depth of invasion, tumor node metastasis (TNM) classification and tumor location.

In the analyses of the association between *F. nucleatum* infection and CRC and the role of hsa-miR-31-5p (miR-31) in *F. nucleatum*-induced colorectal tumorigenesis, we used fresh-frozen CRC tissues obtained from 30 CRC patients (CRC group) and colorectal polyp tissues obtained from 30 patients (Control group) at the Third Affiliated Hospital of Chongqing Medical University (Chongqing, China) from 2016 to 2017. The baseline clinical and pathological characteristics of all specimens were collected (Table S1).

In the analyses of the effects of *F. nucleatum* and miR-31 on RFS, frozen cancer tissues were collected from 109 CRC patients, who were followed up for up to 45 months at the Third Affiliated Hospital of Chongqing Medical University during 2016 and 2020. The baseline clinical and pathological characteristics of all specimens were prospectively collected (Table S2).

In the analyses of potential involvement of STX12 and miRNAs in *F. nucleatum*-associated CRC, we collected fifteen fresh-frozen colorectal cancerous tissue specimens [*F. nucleatum* negative CRC samples (Fn^- CRC, n=5), *F. nucleatum* positive CRC samples at an early stage (Fn^+ early CRC, n=5) and *F. nucleatum* positive CRC samples at an advanced stage (Fn^+ advanced CRC, n=5)] and ten paracancerous colorectal tissue specimens [*F. nucleatum* positive paracancerous samples (Fn^+ control, n=5) and *F. nucleatum* negative paracancerous samples (Fn^- control, n=5)]. These samples were obtained from CRC patients at Southwest Hospital of Army Medical University (Chongqing, China) during 2017 and 2018. Our earlier work, which studied miRNAs and genes implicated in the development of *F. nucleatum*-associated CRC, reported the infection status of tissues and clinical features of CRC patients.[30]

Animal experiments

C57BL/6J wild-type (WT) mice and female BALB/c nude mice were obtained from Beijing Vital River Laboratory Animal Technology. C57BL/6J miR-31 knockout ($miR\text{-}31^{-/-}$) mice were obtained from Shanghai Paizhi Biotechnology Co., Ltd. (Shanghai, China). With autoclaved food and water, mice were raised in specialized pathogen-free conditions. All *in vivo* tests were carried out in accordance with the Army Medical University's Institutional Animal Care (AMUWEC20191778) and Use Committee's approved procedures for the use of laboratory animals.

In the analyses of the association between *F. nucleatum* and CRC tumorigenicity, five/six 5-week-old C57BL/6J WT mice received antibiotics (1 g L^{-1} ampicillin, 0.5 g L^{-1} vancomycin hydrochloride, 1 g L^{-1} neomycin sulfate and 1 g L^{-1} metronidazole) by gavage administration for 3 days, and were given two cycles of one single intraperitoneal injection of carcinogen 10 mg kg^{-1} azoxymethane (AOM; Sigma, St. Louis, MO, USA) followed by five successive days of 3% dextran sodium sulfate (DSS; MP Biomedicals, Shanghai, China) in the drinking water. Then they were administered phosphate-buffered saline (PBS, pH 7.4)-resuspended *F. nucleatum* (10^8 colony-forming units [CFU]) *via* the intestinal tract every day. After 20 weeks, 40 mg kg^{-1} pentobarbital sodium was used to put C57BL/6J WT mice to sleep so they could be killed for tumor and histological studies. Histological examination of the intestinal tissues was performed after hematoxylin and eosin (H&E) staining. The length of the tissues was examined and measured. Tumor counts were conducted, and the diameters of the tumors were classified as follows: 1 mm, 1-3 mm, 3-5 mm, and >5 mm.

In the analyses of the role of miR-31 in *F. nucleatum* promoting CRC tumorigenicity and survival, five/six 5-week-old C57BL/6J WT and $miR\text{-}31^{-/-}$ mice were treated with *F. nucleatum* and then given two cycles of one single intraperitoneal injection of AOM (10 mg kg^{-1}) followed by five successive days of 3% dextran sodium sulfate (DSS; MP Biomedicals) in the drinking water. To investigate the progression of *F. nucleatum*-induced CRC, mice were treated with *F. nucleatum* for 20 weeks and sacrificed for colon appearance and tumor number analysis. To investigate the effects of *F. nucleatum* on survival, mice were followed up until death.

To further investigate whether miR-31 targets STX12 to enhance *F. nucleatum*-induced inhibition of autophagic flux, $miR\text{-}31^{-/-}$ and $miR\text{-}31^{WT}$ mice were first injected with recombinant adenovirus Av-short hairpin RNA (shRNA) (STX12, eIF4EBP1 or eIF4EBP2) (10^9 plaque-forming unit) or negative control (NC) Av-sh NC *via* the tail vein, and then were subjected to *F. nucleatum* and AOM and DSS treatment for 20 weeks. Adenovirus STX12 shRNA or a non-targeting sequence was generated by adenoviral transduction using a pAdeno-Mcmv-Oct-4-EGFP-3FLAG vector (OBiO Co., Ltd., Shanghai, China), as adenovirus shRNA STX12 (Av-sh STX12), adenovirus shRNA eIF4EBP1 (Av-sh eIF4EBP1), adenovirus shRNA eIF4EBP2 (Av-sh eIF4EBP2) or adenovirus shRNA NC (Av-sh NC). Histological examination of the colon epithelium by

H&E staining and colonization analysis of *F. nucleatum* in colorectal tissue by the gentamicin protection assay were performed.

The effects of miR-31 on tumor growth were investigated in tumor xenografts in nude mice. HCT116 cells were infected with Lv-anti-miR-31-5p, Lv-anti-NC, Lv-miR-31-5p, or Lv-NC for 72 h. After 48 h of antibiotic puromycin screening, cells at 70–80% confluence were collected and subcutaneously injected (1×10^7 cells per mouse) into the right flank of 20 6-week-old female BALB/c nude mice (n = 5 per group). The general status and tumor growth of mice were closely monitored at the indicated time points. The mice were euthanized and sacrificed on day 60 and the tumor volumes (Vol) were calculated as follows: Vol=1/2 (length× diameter width^2). Subsequently, the tumor tissues were formalin-fixed and used for Ki-67 immunostaining.

Bacterial strains and cell lines

The *F. nucleatum* strain, *F. nucleatum* subsp. nucleatum ATCC 25586, and *Escherichia coli (E. coli)* DH5α were obtained from the American Type Culture Collection (ATCC, Manassas, VA, USA) and Invitrogen (Carlsbad, CA, USA), respectively. *F. nucleatum* was grown in anaerobe basal broth (Oxoid, Hampshire, UK) in an anaerobic glove box (Anoxomat MarkII anaerobic gas filling system, Mart Microbiology, Netherlands) with 90% N_2, 5% H_2, and 5% CO_2 at 37°C, and *E. coli* DH5α was propagated in Luria-Bertani medium aerobically at 37°C. Four CRC cell lines (SW480, LoVo, HCT116, and HT29), one normal colon epithelial cell line (NCM460), and one human embryonic kidney cell line (HEK293) for the luciferase reporter assay were all provided by ATCC. According to the manufacturer's instructions, all cell lines were cultured under the proper circumstances.

Oligonucleotide construction and lentivirus production

The DNA oligonucleotides containing WT or mutant (MT) 3′ untranslated region (UTR) of eIF4EBP1/2 or STX12 were synthesized with flanking *Spe* I and *Hind* III restriction enzyme digestion sites, respectively. The DNA and pMIR-REPORT™ luciferase vectors (Promega, Madison, WI, USA) were used to construct the luciferase report vectors. The resulting constructs were named pMIR-eIF4EBP1-3′ UTR-WT and pMIR-eIF4EBP1-3′ UTR-MT, pMIR-eIF4EBP2-3′ UTR-WT and pMIR-eIF4EBP2-3′ UTR-MT, pMIR-STX12-3′ UTR-WT and pMIR-STX12-3′ UTR-MT. The sequences of the DNA oligonucleotides are shown in Table S3.

To verify whether p65 can putatively bind to the miR-31 promoter, the promoter of miR-31 was amplified by PCR from HCT116 cells and inserted to the *Mlu* I and *Hind* III restriction enzyme sites of pGL3 Basic Vector (Promega), resulting in the recombinant plasmid pGL3 WT. A QuikChange site-directed mutagenesis kit (Agilent, Shanghai, China) was used to mutate the p65 binding sites, producing pGL3 MT. The sequences of the DNA oligonucleotides are shown in Table S4.

A miRNA mimic, miRNA inhibitor, and control oligonucleotides of miR-31 were purchased from Thermo Fisher Scientific (Waltham, MA, USA). Using the pSLenti-EF1a-EGFP-F2A vector (OBiO Co.), lentiviral transduction was used to create a lentivirus that overexpressed miR-31 or a non-targeting region, as lentivirus-miR-31-5p (Lv-miR-31), or lentivirus-NC (Lv-NC). A lentivirus overexpressing anti-miR-31 or a non-targeting sequence was created by lentiviral transduction using a pLKD-CMV-EGFP-2A vector (OBiO Co.), as lentivirus-anti-miR-31-5p (Lv-anti-miR-31) or Lv-anti-NC. Transfection of lentivirus construction was performed according to the manufacturer's instructions.

A nuclear factor kappa B (NF-κB) p65 shRNA (human) lentivirus (Lv-sh-p65), a STX12 shRNA (human) lentivirus (Lv-sh STX12), and a control shRNA (human) lentivirus (Lv-sh NC) were obtained from Santa Cruz Biotechnology (Shanghai) Co., Ltd (Shanghai, China). Two small interfering RNAs (siRNAs) targeting eIF4EBP1 and eIF4EBP2 (*i.e.,* si-eIF4EBP1 and si-eIF4EBP2, respectively) were synthesized by Sangon Biotech. A sequence without gene targeting was used as a NC (si-NC; Sangon Biotech). Overexpression of eIF4EBP1/2 and STX12 was achieved by transfection with the recombinant TUG1-pcDNA3.1 plasmid containing eIF4EBP1/2 or STX12 (Sangon Biotech). Cells were plated, cultured until the cell density reached 50–60%, and then transfected with the oligonucleotides or recombinant plasmid using Lipofectamine 3000 (Invitrogen) according to the manufacturer's instructions.

METHOD DETAILS

DNA extraction and *F. nucleatum* quantification

Genomic DNA was extracted from human frozen tissues using the QIAamp DNA Mini Kit from Qiagen (Hilden, Germany). By using the Premix EX TaqTM kit (Takara, Tokyo, Japan), *NusG* gene was amplified and identified by qPCR on the CFX96 Real-Time System, with reaction conditions as previously reported.[64] As an internal control, the DNA concentration of the prostaglandin transporter (PGT) reference gene was measured.[6] Table S4 lists the primers and probes for *F. nucleatum* and PGT.

H&E staining

The immunohistochemical staining assay was performed according to our previous report.[64] In summary, tissue sections were cut, dewaxed, rehydrated, and stained with Harris hematoxylin solution. Then, the slices were differentiated, counterstained with eosin, and finally photographed under a microscope.

Immunohistochemistry for Ki-67

The immunohistochemical staining assay was performed according to our previous report.[65] In brief, tissue sections were deparaffinized, rehydrated, repaired with antigen, and blocked. Then the tissue sections were incubated with anti-Ki-67 (ab92742, 1:200; Abcam, Cambridge, MA, USA) and the appropriate secondary antibody, and stained with 3,3′-diaminobenzidine (D12384S, Sigma-Aldrich, Shanghai, China), and photographed after being sealed with neutral glue.

mRNA microarray

HCT116 cells were infected with Lv-anti-NC, Lv-anti-miR-31, Lv-NC, or Lv-miR-31 for 72 h. After 48 h of screening with antibiotic puromycin (Clontech, Palo Alto, CA, USA), the cells in good growth condition with 70–80% confluence were collected. Total RNA was extracted from these cells for RNA microarray with Affymetrix Human Gene 1.0 ST array (GMINIX, Pudong New Area, Shanghai, China).

Luciferase reporter assay

HEK293 cells were co-transfected with the synthetic miR-31 mimic/miR-31 inhibitor/miR-31 control, Lv-shRNA-p65 vector, pGL3 WT or pGL3 MT and the luciferase reporter vectors in 24-well plates using Lipofectamine 3000 reagent (Invitrogen). Following the manufacturer's instructions, luciferase activity was assessed 48 h after transfection using the Dual-Luciferase Reporter Assay System (Promega). The activity of the Renilla luciferase enzyme served as a control. Triplicates of each assay were run independently.

5-Ethynyl-20′-deoxyuridine staining assay for cell proliferation

HCT116 cells were co-cultured with *F. nucleatum* or *E. coli* DH5α for 24 h. Then 10 μM 5-ethynyl-20′-deoxyuridine (EdU) (BeyoClickTM EdU Cell Proliferation Kit with Alexa Fluor 594; Beyotime, Shanghai, China) was added, and the cells were grown for an additional 2 h. The cells were stained according to a previous report.[65] Images were captured under a fluorescence microscope.

Transmission electron microscopy

To detect the autophagosomes, HCT116 cells were co-cultured with *F. nucleatum* (multiplicity of infection [MOI] of 100). To detect the intracellular survival of *F. nucleatum,* HCT116 cells were infected with Lv-sh STX12 or Lv-sh NC, or transfected with the miR-31 mimic, inhibitor or control with or without *F. nucleatum* co-culture. Following treatment, cells were gathered, fixed for 2 h in 2.5% glutaraldehyde in 0.1 M sodium cacodylate buffer, and then fixed for 1.5 h in 1% osmium tetroxide. After being cleaned, cells were stained for 1 h with 3% aqueous uranyl acetate. Cells were dehydrated using a graduated alcohol series and then embedded in Epon-Araldite resin (Canemco, Gore, Canada). An ultramicrotome from Reichert was used to cut extremely thin sections, which were stained with 0.3% lead citrate. The sections were observed by transmission electron microscopy (TEM) (JEM-1400PLUS; Jeol, Tokyo, Japan).

Laser scanning confocal microscopy for detection of autophagic flux

Microtubule-associated protein light chain 3 beta (MAP1LC3B) is widely used to monitor autophagy. To detect autophagic flux, plasmids containing green fluorescent protein (GFP)-MAP1LC3B (GFP-LC3; Addgene) or adenoviruses containing red fluorescent protein-GFP-MAP1LC3B (mRFP-GFP-LC3; Hanheng) were used. For GFP-LC3 fluorescence microscopy, HCT116 cells were transfected with the GFP-LC3

plasmid for 24 h, treated with 100 nM rapamycin (Sigma, USA), 2 mM 3-methyladenine (3-MA) (Sigma, USA), and 10 μM chloroquine (CQ) (Sigma, USA), and then co-cultured with *F. nucleatum* (MOI of 100) for the indicated time points. In tandem mRFP/mCherry-GFP fluorescence microscopy, HCT116 cells were infected with the mRFP-GFP-LC3 adenovirus, treated with rapamycin (100 nM) or bafilomycin A1 (10 nM) (Sigma, USA), and then co-cultured with *F. nucleatum* (MOI = 100) with or without the miR-31 mimic (100 nM) and inhibitor (100 nM) for the indicated time points. Following treatment, cells were gathered and stained for 10 min at room temperature with DAPI (Life Technologies, Frederick, MD, USA). Cover slips were mounted with VECTASHIELD® Mounting Media (H1200; Vector Laboratories, Burlingame, CA, USA). The stained cells were examined using the Zeiss 800 laser scanning confocal microscope (Zeiss, Oberkochen, Germany), and Zen 2012 software was used to conduct additional analysis.

Antibiotics protection assay for assessing *F. nucleatum* infectivity

HCT116 cells infected with *F. nucleatum* were washed three times with PBS and incubated with fresh culture medium containing gentamicin (Sigma, USA) (100 μg/mL) and metronidazole (MTZ) (Sigma, USA) (200 μg/mL) for 1 h to kill extracellular and epithelial cell surface-bound bacteria. After being washed three times with PBS, the cells were lysed at 37°C for 15 min with 1 mL of 0.5% saponin (Sigma, USA). Diluted cell lysates were plated on Anaerobe Basal Broth plates (Oxoid, Basingstoke, Hants., UK). Colonies were counted after 48 h. On the other hand, the infected monolayers were treated with 1 mL of 0.5% saponin in PBS at 37°C for 15 min without prior treatment with gentamicin and metronidazole in order to ascertain the total CFU corresponding with host-associated bacteria. As previously mentioned, the resultant suspensions were diluted and plated. Both the total CFU of cell-associated bacteria and the CFU of intracellular bacteria are given as CFU/ml of HCT116 cells. The experiments were performed at least three times in triplicate.

Cell proliferation and colony formation assays

The proliferation of HCT116 and LoVo cells with or without treatment was assessed using Cell Counting Kit-8 (CCK-8; Beyotime, Shanghai, China) according to the manufacturer's instructions. In brief, cells were seeded at a density of 2000 cells/well in a 96-well plate and treated with 10 μL/well of CCK-8 for 2 h at 6, 24, 48, 72, and 96 h post-seeding. Cell proliferation curves were plotted using the 450 nm absorbance measured at each time point. For the colony formation assay, 800 cells were seeded in a 6-well plate and maintained for 12 days. Visible colonies were dyed by 50% crystal violet and counted. All assays were performed in triplicate.

RNA extraction and qRT-PCR analysis

The TRIzol reagent (Invitrogen) was used to extract total RNA from tissue samples and the treated CRC cells. According to the manufacturer's instructions, cDNA was generated using the TaqManTM microRNA Reverse Transcription Kit and then subjected to qPCR using the TaqManTM MicroRNA Assay Kit from Applied Biosystems. The qPCR was performed as follows: 95°C for 2 min and 40 cycles of 95°C for 15 s and 60°C for 30 s. U6 small nuclear RNA was used as an endogenous control. The comparative threshold cycle method was used to compute the relative expression.[30] The mRNA expression of STX12 and pri-miR-31 was detected with PrimeScript RT-PCR kits (DRR037; Takara) in qRT-PCR analyses. The mRNA level of GAPDH was used as an internal control. The reaction parameters were as follows: 95°C for 2 min, followed by 39 cycles of 95°C for 15 s and 60°C for 30 s. The primers used are presented in Table S5.

Preparation of soluble and insoluble SQSTM1

The T-PER™ Tissue Protein Extraction Reagent (Thermo Fisher Scientific) combined with the Halt™ protease inhibitor cocktail (Thermo Fisher Scientific) was used to lyse the HCT116 cells. The lysate was centrifuged at 17,000 × g for 20 min at 4°C, and the supernatant was recovered as a detergent soluble fraction as previously described.[66] The insoluble pellet was dissolved in T-PER™ Tissue Protein Extraction Reagent supplemented with 2% sodium dodecyl sulfate and centrifuged at 17,000 × g for 20 min at 4°C. The supernatant was separated into insoluble fractions. The concentration of each protein fraction was determined using the BCA protein assay (Merck, Shanghai, China) and analyzed using western blotting.

Western blotting

The T-PER™ Tissue Protein Extraction Reagent (Thermo Fisher Scientific) combined with the Halt™ protease inhibitor cocktail (Thermo Fisher Scientific) was used to lyse tissues and cells. The nuclear and

cytoplasmic protein extraction kit (P0027; Beyotime Biotechnology, Shanghai) was used to extract the cytosolic and nuclear fractions, as directed by the manufacturer. Proteins were separated on polyacrylamide gel electrophoresis with 10% sodium dodecyl sulfate and electrotransferred onto polyvinylidene fluoride membranes (Millipore, Burlington, CA, USA). The membranes were blocked in 5% fat-free milk before being treated with the primary antibodies listed below: STX12 (SAB1400469) and MAP1LC3B-I/II (L7543) antibodies were purchased from Sigma (USA); GAPDH (5174S), Phospho-NF-κB p65 (3033T), SQSTM1/p62 (5114S), eIF4EBP1 (9644S), and eIF4EBP2 (2845S) were from Cell Signaling Technology (Danvers, MA, USA). All horseradish peroxidase-conjugated secondary antibodies (7076P2, 7074S) were purchased from Cell Signaling Technology (USA). The protein bands were photographed using imaging equipment after being visualized using enhanced chemiluminescence according to the manufacturer's directions.

Chromatin immunoprecipitation

The chromatin immunoprecipitation (ChIP) assay was performed using the ChIP Assay Kit (Beyotime, China) according to the manufacturer's instructions. Briefly, HCT116 or LoVo cells were cross-linked with 1% formaldehyde, collected, lysed, and sonicated to shear DNA. Then the DNA-protein complexes were isolated with antibodies against p65 (8242, Cell Signaling Technology, Shanghai, China), or isotype IgG (3900S, Cell Signaling Technology). The protein/DNA complexes were then eluted and reverse cross-linked, and the DNA was purified by spin columns. The precipitated DNA was quantified by polymerase chain reaction, and the primers used are listed in Table S6.

QUANTIFICATION AND STATISTICAL ANALYSIS

For continuous data, the Mann-Whitney U test was used to compare two groups, an unpaired or paired Student''s t-test was used to compare several groups, and one-way analysis of variance was used to compare several groups. The relationships for continuous data were carried out either using Fisher's exact or Pearson's chi-squared tests. The impacts of the clinical parameters presented in Tables S1 and S2 on prognosis were estimated using univariate or multivariate Cox proportional hazards regression. For RFS analyses, Kaplan-Meier analysis and the log-rank test were used. All *P* values were two-tailed, and statistical significance was defined as $P < 0.05$. All statistical analyses were conducted using GraphPad Prism 6 and IBM SPSS Statistics 20.0.